https://doi.org/10.1016/j.cemconres.2021.106462

Citation: Jian-Xin Lu, Peiliang Shen, Haibing Zheng, Hafiz Asad Ali, Chi Sun Poon*,Development and characteristics of ultra high-performance lightweight cementitious composites (UHP-LCCs), Cement and Concrete Research 145 (2021) 106462. https://doi.org/10.1016/j.cemconres.2021.106462

Development and characteristics of ultra high-performance lightweight cementitious composites (UHP-LCCs)

Jian-Xin Lu, Peiliang Shen, Haibing Zheng, Hafiz Asad Ali, Chi Sun Poon*

Department of Civil and Environmental Engineering, The Hong Kong Polytechnic University,
Hung Hom, Kowloon, Hong Kong, China

*Corresponding author: cecspoon@polyu.edu.hk

Abstract: High strength and light weight are two recent opposite development trends of concrete. This study proposed a design concept of an ultra high-performance lightweight cementitious composite (UHP-LCC), which had a compressive strength of higher than 120 MPa and an air-dried density down to around 1,800 kg/m^3. The UHP-LCCs were innovatively developed by incorporating micro-sized hollow particles with a high strength shell (hollow glass microspheres, HGM) into an ultra-high performance cementitious composite (UHPC). The roles of HGM in the UHP-LCCs were investigated by evaluating the reactivity of the HGM and the mechanisms on achieving the excellent mechanical properties, low density and superior durability were revealed. The Chapelle test results showed that the HGM exhibited some pozzolanic reactivity, which facilitated the reaction between the shell of HGM and the alkali hydration products of the paste matrix. This chemical reaction was conducive to improving the HGM-paste interface and enhancing the mechanical properties. With the use of microspheres with a high stiff shell, the fundamental properties of the UHP-LCCs including thermal insulation, sound absorption, resistance to water ingress and electrical resistivity were improved significantly. The strategies for preparing the UHP-LCCs with high structural efficiency and great performance were proposed. The results of this study provide a new approach for designing and producing a lightweight UHPC, which would be a promising material for long-span structures.

Keywords: Lightweight UHPC; Lightweight cementitious composite (LCC); Hollow glass microspheres (HGM); Ultra high strength; Structural efficiency

1 Introduction

High strength and light weight are two important trends of concrete development. However, how to balance these two characteristics and produce a higher structural efficient (strength/weight) concrete remains a challenge. High strength and light weight seem to be opposite as the strength of concrete generally decreases with decreasing density. But, in recent years, with the increasing demand of super high-rise buildings, long-span bridges and offshore platforms, the practical need for the development of high strength lightweight concrete is increasing. This is especially necessary for the rapid development of the use of modular integrated construction, as the use of high strength lightweight concrete is beneficial to increasing lifting efficiency, reducing transportation costs and improving sound insulation. Except being lightweight and high strength, other advantages of the high strength lightweight concrete have been reported when compared to conventional concrete, such as good thermal insulation, better durability, and cost saving [1, 2].

The common methods for producing lightweight concrete are to incorporate air/bubbles or lightweight aggregates. In comparison with concrete prepared with lightweight aggregates, the lightweight concrete containing voids/bubbles usually has low mechanical properties, which is not suitable to be used in concrete structures. Hence, the introduction of lightweight aggregates is considered as a more effective approach to both reduce the weight of concrete and enhance the strength for structural applications. Lightweight aggregates can be roughly classified into (i) natural aggregates (e.g. pumice and scoria), (ii) artificial aggregates (e.g. expanded clay and shale) and aggregates recycled from wastes (e.g. palm oil clinker and coconut shell), and generally have a bulk density of less than 1200 kg/m^3. By means of incorporating silica fume and high-range water reducer, structural high strength lightweight aggregate concrete (HSLAC) could be produced, which typically exhibits compressive strength higher than 40 MPa and density less than 2000 kg/m^3 [3-5].

The investigations on HSLAC have attracted many researchers’ interests. Zhang and Gjørv [6] found that the compressive strength of HSLAC was primarily controlled by the type of lightweight aggregates, whereas the lightweight aggregates were not the dominant factor in affecting the permeability of HSLAC [7]. A dense mortar matrix in the HSLAC was able to induce a lower permeability comparable to normal weight concrete at the same level of strength [7]. One breakthrough finding of their work was the successful preparation of HSLAC with a compressive strength of up to 100 MPa and a density down to 1,865 kg/m^3 [6]. However, the corresponding tensile strength of these HSLAC was still lower than that of normal weight concrete [6]. Thus, steel or polypropylene fibers were incorporated to increase the tensile and flexural strength of the HSLAC [8, 9]. Although the inclusion of porous aggregate into HSLAC would increase the total porosity of the concrete, comparable or even superior durability performances (lower water sorptivity and permeability, and chloride ion penetration) could be obtained in comparison with normal weight concrete [10]. When the HSLAC was prepared with dry lightweight aggregates, its ultimate shrinkage was larger than that of normal weight concrete due to the lower modulus of elasticity of the lightweight aggregates. When pre-soaked lightweight aggregates were incorporated, the HSLAC could experience lower shrinkage and creep than normal high performance concrete [11]. The internal curing effect from the pre-wetted aggregates was thought to mitigate the autogenous shrinkage and the drying shrinkage [12-14]. It was also reported that the incorporations of steel fiber and silica fume could reduce the shrinkage of HSLAC [12]. Similar results were found by Chen and Liu [15], who indicated that the addition of hybrid fibers could effectively reduce the shrinkage, enhance the compressive and splitting tensile strengths, and reduce the brittleness of HSLAC. Moreover, they suggested to use a combination of supplementary cementitious materials (e.g. fly ash and silica fume) in HSLAC to avoid bleeding/segregation or inferior workability [16]. The benefits of using pozzolanic admixtures were also reported in another study [17], which showed that the use of silica fume and metakaolin could improve the mechanical properties and durability of HSLAC, such as increases of tensile strength and modulus of elasticity, reductions of chloride permeation and corrosion rate, increase of carbonation resistance. In order to improve the durability of HSLAC, Atmaca et al. [18] used nano-silica as a replacement of cement to counteract the negative impacts caused by the use of pelletized lightweight aggregates. Given the HSLAC could achieve equal or superior long-term strength and durability to the conventional concrete, it has been applied for the construction of concrete girders, bridges, high-rise buildings, marine structures [19-22].

However, the above HSLAC produced mostly have unit weights ranging from 1,800 to 2,000 kg/m^3 and compressive strength of around 40-70 MPa. It is of scientific interest and great practical need to explore the possible production of high strength cement composites with a higher structural efficiency (i.e. higher strength and lower density). Previously, researchers focused mainly on producing UHPC via maximizing the packing density (expelling air voids as much as possible) [23-26], or producing ultra lightweight composites by the use of low density materials (entrapping pores as much as possible) [27-31]. These two aspects seem to be contradictory and are not conducive for producing ultra high strength lightweight cementitious composites. Recently, some studies attempted to introduce a small volume of lightweight aggregates in the UHPC system for reducing autogenous shrinkage (internal curing effect) [32-36] rather than toward weight reduction. Therefore, this study aims to develop an ultra high strength and super lightweight cement composite. A summary of past research and differences with this study are presented in the following Table.

Table 1 Summary of comparison between the past studies and this study.

References	System	Objective	Density (kg/m^3)	Compressive strength (MPa)
This study	Ultra high-performance lightweight cementitious composite (UHP-LCC) incorporating micro-sized voids with a high strength shell	Achieving ultra high strength of above 120 MPa and density value less than 1,920 kg/m^3	< 1,920	> 120
[23-26]	UHPC including silica sand	Achieving strength as high as possible by maximizing packing density	Normally > 2,400	> 120
[27-31]	Ultra lightweight composites including lightweight materials	Achieving density as low as possible by using low density materials	500~1,400	5~30
[32-36]	UHPC including lightweight aggregates	Reduction of autogenous shrinkage	> 2,300 in [33]	> 100

Currently, no investigation has been reported regarding the preparation of lightweight cementitious composites with a compressive strength of above 120 MPa (lower limit of UHPC in ASTM C1856C [37]) and with density value less than 1,920 kg/m^3 (upper limit of structural lightweight concrete in ACI 213R [38]). One important factor may be related to the performance of fine lightweight materials included. Therefore, this study firstly proposed the design concept of an ultra high performance lightweight cementitious composite (UHP-LCC) in terms of terminology and definition, and then conducted experimental studies to produce the UHP-LCCs by introducing a large amount of micro-sized voids with a high strength shell. To this end, high performance hollow glass microspheres (HGM) were selected and incorporated in UHP-binder to ensure the lightweight characteristic, ultra high strength and excellent durability. The roles of HGM in the UHP-LCCs were revealed by evaluating its pozzolanic reactivity, physical structure and mineralogy. Also, the physical, functional and durability properties of the UHP-LCCs were evaluated and analyzed. The mechanisms and strategies on achieving the good performance of the UHP-LCCs were discussed based on multiple microstructure techniques.

2 Materials and methods

2.1 Materials

An ordinary Portland cement (CEM I 52.5) produced by Green Island in Hong Kong was used as a main cementitious material. Silica fume (SF) and HGM were sourced from Mainland China. The HGM was incorporated in the cementitious composite for weight reduction. In this study, the HGM was produced by spraying-granulating-heating method from an aqueous glass precursor solution. Glass powder (GP) derived from crushing and grinding recycled beverages glass bottles was employed as a filler in the mixture. The glass bottles were produced by melting-moulding-annealing procedure from solid raw materials (such as quartz sand, sodium carbonate, limestone, etc.). A straight steel fiber (density of 7.8 kg/m^3, diameter of 0.22 mm and length of 13 mm) coated with copper was used. A high efficiency polycarboxylate superplasticizer (SP, BASF) was used for water reducing. The chemical compositions of the cementitious materials and the HGM are listed in Table 2, which were determined by X-ray fluorescence spectrometer (Rigaku Supermini200). It should be noted that the SF, GP and HGM were silica-rich materials, especially the GP and the HGM had a similar composition, rich in SiO_2, CaO and Na_2O. The particle size distributions (PSD) of the cement and GP were measured by a laser diffraction particle size analyzer (Malvern Mastersizer 3000E). Due to the extremely fine size of SF, its PSD was determined by Zetasizer (Malvern, Nano-ZS90) after ultrasonic dispersion in ethanol. The PSD results in Fig. 1 show that the cement particles were much larger than the SF, but finer than the GP particles.

Table 2. Chemical compositions of materials (wt. %).

Compositions	Cement	SF	GP	HGM
SiO_2	19.0	95.7	69.0	80.5
Al_2O_3	5.68	0.45	2.62	0.86
CaO	65.8	0.73	10.5	8.36
MgO	0.97	0.71	1.35	0.14
K_2O	0.66	1.74	0.79	0.08
P_2O_5	0.16	0.09	0.12	0.09
Fe_2O_3	3.12	0.07	1.42	0.06
Na_2O	-	-	13.5	9.71
SO_3	4.03	0.27	0.13	0.19
Physical properties				
Density (g/cm^3)	3.15	2.58	2.40	0.42
Average particle size (μm)	22.7	0.44	47.0	36.3

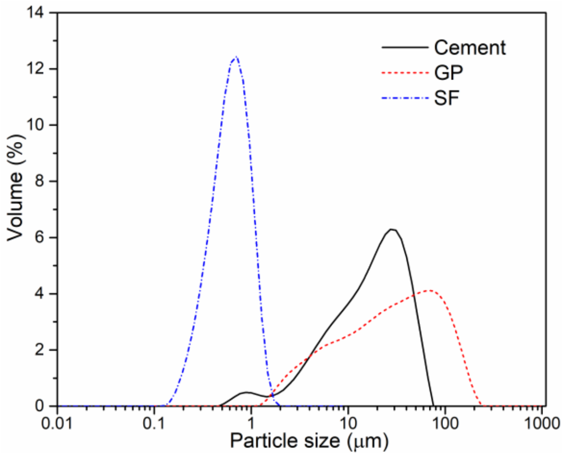

Fig. 1. Particle size distributions of cement, SF and GP.

2.2 Design concept and characteristics of HGM

2.2.1 Design concept

This study aims to develop an ultra high-performance lightweight cementitious composite (UHP-LCC) with a view to achieving high strength (＞120 MPa [37]) and light weight (＜ 1,920 kg/m^3

[38]). To realize this target, the cement matrix should have a very high strength and the lightweight media should have a very low density. Therefore, for the matrix, an UHPC binder was employed as the main cementitious binder. As known, a typical UHPC can exhibit excellent strength (＞ 120 MPa [37]) thanks to its dense structure, but the density of this matrix would be high. It is very crucial to select the type of lightweight materials to achieve the low-density target. Several principles for the selection of lightweight materials were taken into account: (i) as the lightweight materials would be hollow or porous, they should have a high strength and low apparent density; (ii) due to the low water to binder (*w*/*b*) ratio used for the ultra high performance mixture, the lightweight materials should not absorb too much water; (iii) to obtain a good workability, the lightweight materials selected are preferred to have a spherical shape; (iv) lightweight materials with pozzolanic reactivity are preferred as this would improve the bonding between them and the paste matrix. Based on the above principles, a HGM with a high gas isostatic compression strength (20.7 MPa) was chosen as the lightweight media in the production of UHP-LCCs. The characteristics of the HGM will be reported in the following part.

2.2.2 Characteristics of HGM and GP

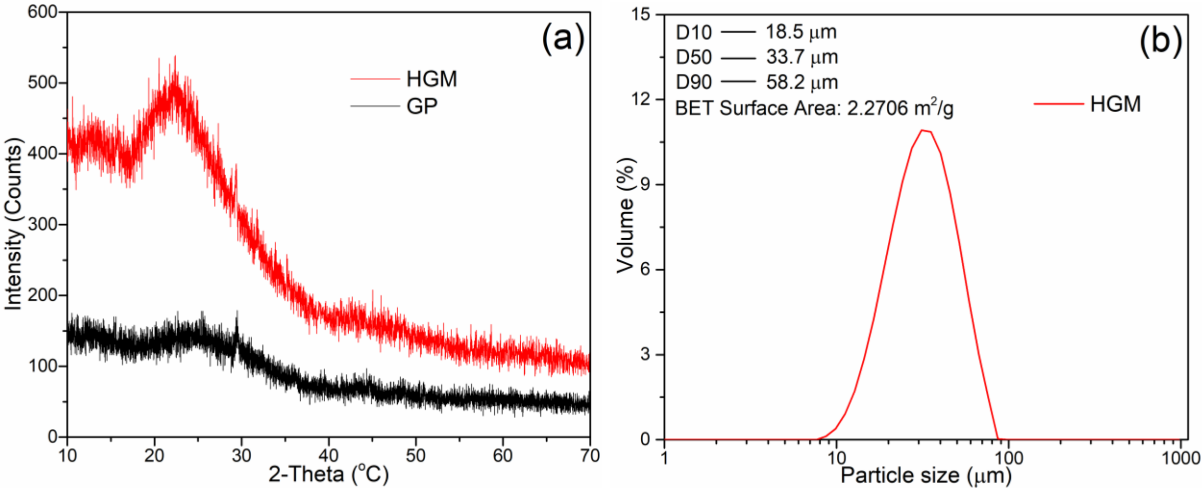

Fig. 2. (a) XRD patterns of HGM and GP; (b) Particle size distribution of HGM.

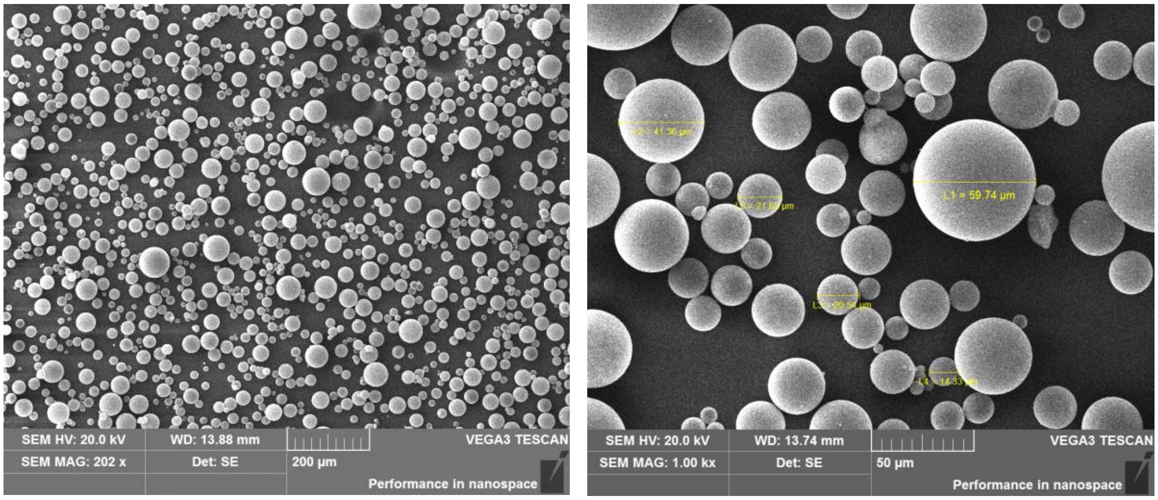

Fig. 3. Morphologies of HGM.

The crystallinity of the HGM was determined by X-ray diffraction (XRD) analysis (Fig. 2a). In comparison with the GP, the HGM also possessed a similar non-crystalline structure. The PSD of the HGM in Fig. 2b shows that the particle size of HGM mainly concentrated in the range of 10-100 μm with an average size of 36.3 μm. As indicated in our previous work [39], GP with a similar particle size exhibited a satisfactory pozzolanic reactivity. As the composition and the vitreous structure of the HGM were similar to those of GP, it is believed that the HGM would also have some pozzolanic reactivity in the cementitious system. The morphologies of the HGM were observed by scanning electron microscopy (SEM, Tescan VEGA3). The images presented in Fig. 3 show that the HGM had spherical shapes with a smooth surface. Whereas, the normal-weight GP (2,400 kg/m^3) had a solid structure with angular shapes as shown in [39]. It is noted that the HGM spheres were micro-sized and non-broken. The glass-based structure, smooth texture and intact microsphere would result in low water absorption, while the ball-like microspheres are expected to benefit the workability due to the lubricating effect. As the HGM was hollow and fine-sized, its apparent density was quite low (420 kg/m^3) and the surface area was high (2.27 m^2/g). Thus, the main purpose of adoption of the HGM was to reduce the weight of the proposed cementitious composite by means of its low density. The characteristics of the HGM accorded closely with the proposed principles for the preparation of the ultra high-performance lightweight composites. As the GP was a solid waste, one aspect of using it was to eliminate the use of quartz powder or other natural fillers in the UHPC matrix. Due to the non-water absorbing nature and pozzolanic reactivity of GP, the other aim of using GP was to improve the performance of UHPC matrix as both a filler and a supplementary cementitious material

(SCM).

2.3 Mix proportions and research framework

In this study, the main cementitious materials in the UHPC binder were cement, SF and GP. The cement had the highest density (see Table 2). Moreover, it is generally known that the degree of hydration of cement in the UHPC binder is very low due to the extremely low water content in the system [40, 41]. Therefore, a large amount of cement would be "wasted" or just act as an "expensive" filler in the mixture. Based on this, the HGM was introduced in the mix design to replace part of the cement with a view to reducing the density of the matrix. The replacement ratios were 0%, 10%, 30%, 50% by volume. The mixtures were codified as Ref, 10C, 30C and 50C, respectively. Furthermore, considering the particle size and chemical composition of GP were similar to those of HGM, attempts were made to fully replace the GP by the HGM (by volume). The replacement of GP by HGM was used in the 50C mix to further reduce the weight of sample (coded as 50C100G). The mix proportions are listed in Table 3. For all the mixtures, the volume of steel fiber used was set to 1.5% by volume, the SP dosage was at 3% of binder mass [42]. As the incorporation of the HGM could increase the workability due to the ball-bearing effect, the amount of water used was adjusted to obtain a similar self-flow spread (195±5 mm).

For the preparation of samples, the dry powder materials were pre-mixed for 3 mins in a laboratory mixer. Then, the SP and water were added into the mixer for another 3 mins' mixing at a slow speed, followed by mixing at a high speed for 6 mins. Finally, the steel fiber was introduced to obtain a homogenous mixture after 2 further mins' mixing at a slow speed. Then, the workability of the fresh mixtures was measured in a flow table [43] and then the mixtures were cast into steel moulds, followed by vibrating using a laboratory vibrating table for 30 s to compact the fresh mixtures. Plastic sheets were used to cover the surface of the samples to avoid moisture loss. After 24 hours, the samples were demoulded and transferred to an 80 ^{o}C chamber for steam curing for 48 hours as recommended [44].

Table 3. Mix proportions of this study (kg/m^3).

Mix	Cement	SF	GP	HGM	Steel fiber	Water	SP	*w/b*
Ref	1523	229	229	0	130	230	60	0.140
10C	1371	229	229	20	130	191	60	0.129
30C	1066	229	229	61	130	158	60	0.130
50C	762	229	229	102	130	135	60	0.138
50C100G	762	229	0	140	130	130	60	0.157

Note: The water content in the SP was 80%.

The study was then divided into three parts. The first part was to determine the reactivity of HGM in order to understand its role in the UHP-LCCs. The Chapelle test associated with the thermal analysis and SEM observations were used in the first part. The second part intended to evaluate the effects of the HGM inclusion on the properties of the UHP-LCCs, including physical properties (density, mechanical properties), functional properties (thermal conductivity, sound insulation) and permeability (electrical resistance, water sorptivity). The microstructure analyses of the UHP-LCCs were explored in the third part, which attempted to reveal the mechanisms on achieving the high strength and light weight for the UHP-LCCs prepared with the HGM.

2.4 Methods

2.4.1 Chapelle test

In order to understand the pozzolanic reactivity of the HGM at high temperature (steam curing condition), the Chapelle test was conducted to compare the pozzolanic activity of HGM, GP and SF following the same procedures reported previously [45, 46]. As the HGM was used to replace the GP by volume, in this test, the same volume of pozzolanic materials was used. Thus, 0.17 g of HGM, 1 g of GP and 1.08 g of SF were added separately into 200 mL distilled water to react with 1 g of $Ca(OH)_2$ (CH). The remaining and reacted CH amounts could be obtained based on the consumed HCl dosage. The reactivity of HGM, GP and SF could also be calculated: the consumed CH amount by materials divided by the original CH amount. After reaction, solid residues dried at 60 °C were measured by thermogravimetric (TG) analysis. The bound water of the residues (excluding portlandite) could be calculated from the mass difference between 105 °C and 350 °C [47].

2.4.2 Density and mechanical properties

Samples with dimension of 40×40×160 mm^3 were prepared for density and mechanical properties measurements. After steam curing for 48 hours, the samples were taken out and cooled down to room temperature with covering by a wet towel. Then, the volumes of the samples were tested by a water displacement method according to BS EN 12390-7:2019 [48]. Thus, the density could be calculated: the mass of the samples in the air divided by the volume (including the internal pores). It should be noted that the density determined was the air-dried density (not oven-dried density). The flexural strength of the samples was carried out by a centre-point loading method according to BS EN 12390-5:2019 [49]. The loading rate for the flexural strength was 0.5 mm/min. The fractured specimens were further subjected to compressive loading on the cross-sectional area at a rate of 0.6 MPa/s to obtain the equivalent compressive strength. The measurement was conducted in accordance with BS EN 12390-3:2019 [50]. The average values were obtained by measuring at least three samples. In order to produce more sustainable and economical products, samples cured under standard conditions for 112 days (water curing at 23±2 °C) were also used to determine the density and the mechanical properties.

2.4.3 Thermal conductivity

A thermal conductivity meter (Hot Disk M1) with a range of 0.03 to 40 W/m/K was employed to measure the thermal conductivity of the samples. The device was equipped with a Hot Disk Kapton sensor 8563 (radius 9.9 mm). The samples for thermal conductivity tests were of dimension of 40×40×40 mm^3. The testing time was 40s for one measurement. The testing temperature was controlled at 21 °C. For each mix, 10 values were obtained to calculate the average result.

2.4.4 Acoustic properties

The equipment used for testing the sound absorption of samples was an impedance tube (Brüel & Kjær, Denmark), complying with ASTM E1050-19 [51]. The sound transmission loss (TL) of the samples was also measured by the impedance tube using four-microphone transfer-function method according to ASTM E2611-19 [52]. The samples prepared for these two measurements were secant circular slices with a diameter of 98 mm and a thickness of 25 mm. Prior to the test, the samples were pre-dried at 40 °C for 3 days to remove moisture in the surface pores. The gaps between the sample and the tube were sealed by blu-tack to prevent noise leakage. The sound absorption coefficients (α_n) and TL were recorded at the frequency range from 0 to 1600 Hz (large tube mode). An analysis system with multi-channel digital frequency was equipped in a computer for data acquisition and processing. Two samples were tested for obtaining an average result.

2.4.5 Electrical resistivity

The electrical resistivity is a property of the cementitious material associated with the corrosion of reinforced concrete, and a high resistivity generally indicates a low risk of corrosion, and vice versa [53]. In this study, electrochemical impedance spectroscopy (EIS) was employed to determine the bulk electrical resistance of the samples. The samples with the dimension of 40×40×40 mm^3 were clamped tightly by two electrodes. A Multi-Autlab M 204 was used for the electrochemical measurement. The frequency chosen in the EIS tests was ranged from 100 kHz to 10 mHz. A 10 mV AC signal magnitude was performed. The EIS results were analyzed by a ZsimpWin software. Nyquist plots can be obtained in the EIS measurement, as shown in Fig. 4. A bulk arc and an electrode arc constitute the impedance spectrum. The connection point of bulk arc and electrode arc is defined as the value of bulk electrical resistance (R_b). Thus, the electrical resistivity (E_r) of the samples can be calculated by the following equation.

$$E_r = \frac{R_b S}{L}$$

Where:

E_r is the electrical resistivity (Ω·m);

R_b is the bulk electrical resistance (Ω);

S is the cross-sectional area of the sample (m^2);

L is the length of the sample (m).

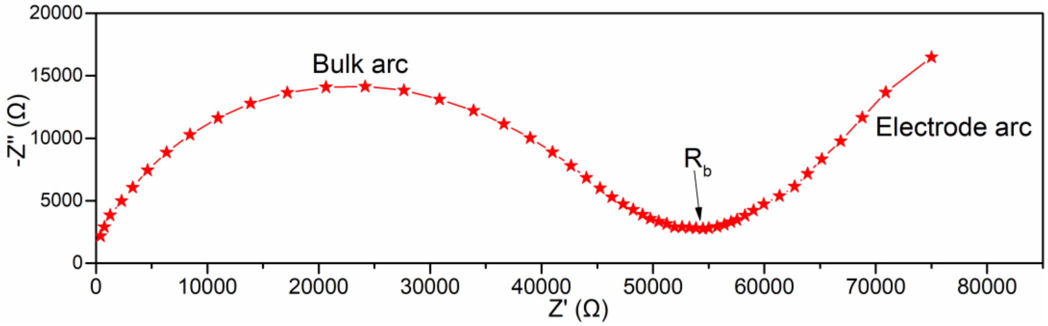

Fig. 4. A typical Nyquist plot obtained from EIS, Real impedance (Z') and Imaginary impedance (-Z")

2.4.6 Water sorptivity

The water sorptivity was determined to evaluate the susceptibility of the samples to water ingress. The test method was performed complying with ASTM C1585-13 [54]. After 48 hours steam curing, the samples were cut into slices with disc diameter of 100 mm and thickness of 25 mm, followed by drying them in a 50 ºC chamber until reaching constant mass. Since the samples had very low water absorption, the procedure was conducted up to 49 days at room temperature (23±2 °C).

2.4.7 Microstructure tests

After steam curing for 48 hours, the samples were cut into thin slices and immersed into anhydrous ethanol to stop further hydration. Then, the small slices were dried in a 60 ºC vacuum oven to remove the residual ethanol. For X-ray diffractometer (XRD) and TG measurements, the dried slice samples were ground into powder to less than 63 μm. The steel fibers in the samples were taken out by a magnet. For SEM/backscattered electron (BSE) imaging test, the slice samples were embedded in epoxy resin firstly and then were ground by a polisher with different grits of papers (320, 600, 1200 grits) step by step to uncover the epoxy attached on the surface of samples. Afterward, further 5 mins polishing was conducted with finer diamond papers (grits 9 μm, 3 μm, 0.05 μm) to obtain smoother surfaces, respectively. Then, the samples were dried at 60 ºC vacuum oven until testing. For Brunauer-Emmett-Teller (BET) test, the slice samples were crushed into small fragments with size in the range of 1.18-2.36 mm. Also, the steel fibers in the samples were removed.

XRD (Rigaku SmartLab) was applied to identify the crystalline phases in the samples. The XRD was equipped with 9 kW rotating anode X-ray source (λ~1.54Å). Bragg-Brentano focusing mode was adopted to determine the powdered samples by using a scan speed of 3°/min and a step size of 0.01°. The scan range (2θ) in the measurement was set from 5º to 75º. To quantify the crystalline phases in the samples, 10 wt% of crystalline Al_2O_3 was mixed with the powdered samples as the internal standard. Rietveld refinement was performed by using Topas 4.2 software to analyze the quantitative XRD (Q-XRD) results. TG/DTG analysis was also carried out by using a Rigaku Thermo Plus EVO2. Around 10 mg sample was weighted for testing. The samples located in corundum crucibles were measured from 30 to 1000 ºC at a heating rate of 10 ºC/min. Argon gas was selected as the testing environment.

For the SEM/BSE observation, the polished bulk samples and fractured samples were respectively coated by carbon and gold first for conduction. Then the surface was observed by a tungsten thermionic emission SEM (Tescan VEGA3) equipped with energy dispersive X-ray spectroscopy (EDX) detector. For the powdered samples, the surface morphologies were observed in the secondary electron mode by SEM. The powders were attached on a conductive adhesive and coated by gold. Both SEM and SEM/BSE measurements were carried out at 20 kV voltage and a working distance of 10-17 mm. For the BET test, nitrogen adsorption and desorption isotherms were monitored by a porosimetry instrument equipped with a two-station degas system (Micromeritics ASAP 2020). Around 0.5 mg sample was used for the measurement. After degassing at 60 °C, analysis procedure was conducted to obtain the pore information in the range of 2-100 nm.

3 Experimental results

3.1 Reactivity of pozzolana

3.1.1 Chapelle test

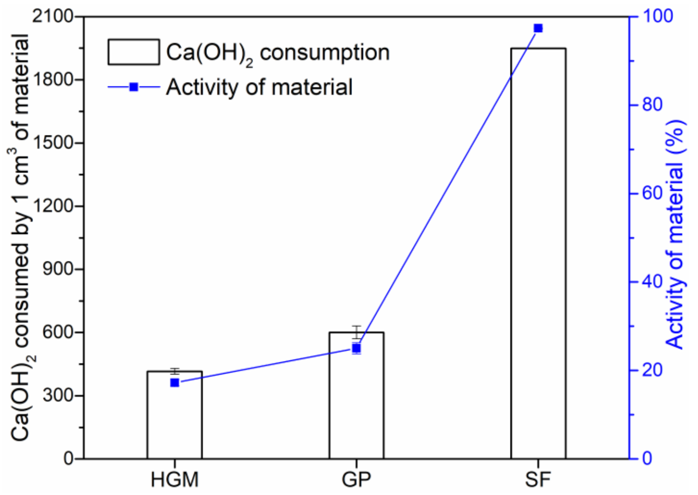

Fig. 5. Ca(OH)$_2$ consumption of HGM, GP and SF in the Chapelle tests.

The portlandite consumption results of the tested pozzolana in the Chapelle tests are shown in Fig. 5. It can be seen that the HGM consumed the smallest amount of CH, corresponding to the lowest activity amongst the three materials tested. The GP showed a slightly higher CH consumption and activity. In comparison with the HGM and GP, the SF consumed almost all the CH, thus its activity index approached to nearly 100%. This means that the SF with an extremely fine particle size possessed the highest pozzolanic reactivity. The GP with a lower reactivity had been classified as a moderately-reactive SCM [46], which was also confirmed by the relatively lower early strength of GP-containing mortar [55]. Nonetheless, the role of the GP was not only a filler, and it potentially acted as a SCM in the UHP-LCCs, especially under the steam curing condition. Similarly, the HGM with a vitreous structure would also exert a moderate pozzolanic reactivity.

3.1.2 TG and SEM analyses

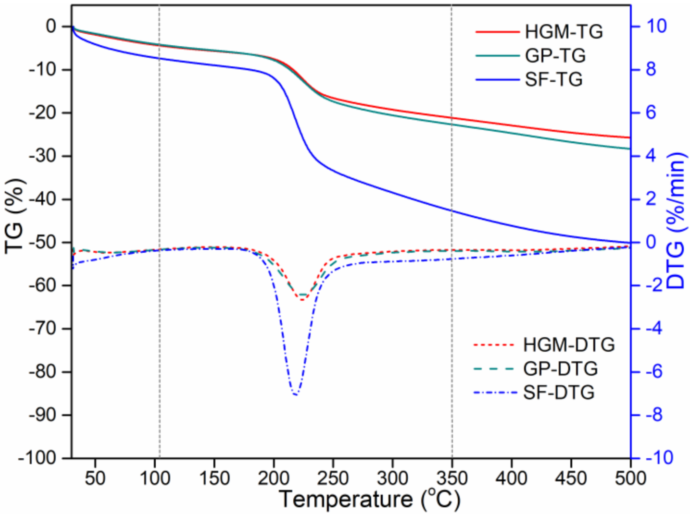

Fig. 6. TG and DTG curves of the solid residues in the Chapelle test.

The TG/DTG results of the solid residues after the Chapelle test are presented in Fig. 6. As seen, the residue of SF sample had a much higher mass loss than the HGM and GP samples, which indicates a higher amount of hydrates in the SF sample. This is consistent with the highest CH consumption of the SF sample shown in Fig.5. Also, the calculated amounts of bound water of the SF, GP and HGM samples were 35.3%, 18.4%, 16.7%, respectively. Hence, the bound water contents of the HGM and GP residues were similar, which are also consistent with their comparable consumptions of CH.

Fig. 7a demonstrates the morphological images of HGM exposed to the saturated CH solution for 28 days. Obviously, the spherical surfaces became rougher as compared to the raw HGM presented in Fig. 7c. A closer examination of Fig. 7b further shows the formation of hydration products on the surface of the HGM. Since the HGM was rich in SiO_2, it is suggested that the amorphous SiO_2 could react with the CH to form calcium silicate hydrates (C-S-H) gel after experiencing the CH attack. The EDX result in Fig. 7d shows a higher amount of calcium on the corroded surface of the HGM. The Ca/Si ratio was 0.41 at the yellow point, which is much higher than the Ca/Si value of the raw HGM (0.16). This indicates the formation of C-S-H gel when the HGM was exposed to CH environment. Hence, it is believed that the pozzolanic reaction between the HGM and the alkaline hydration products would also occur in the cement-based matrix.

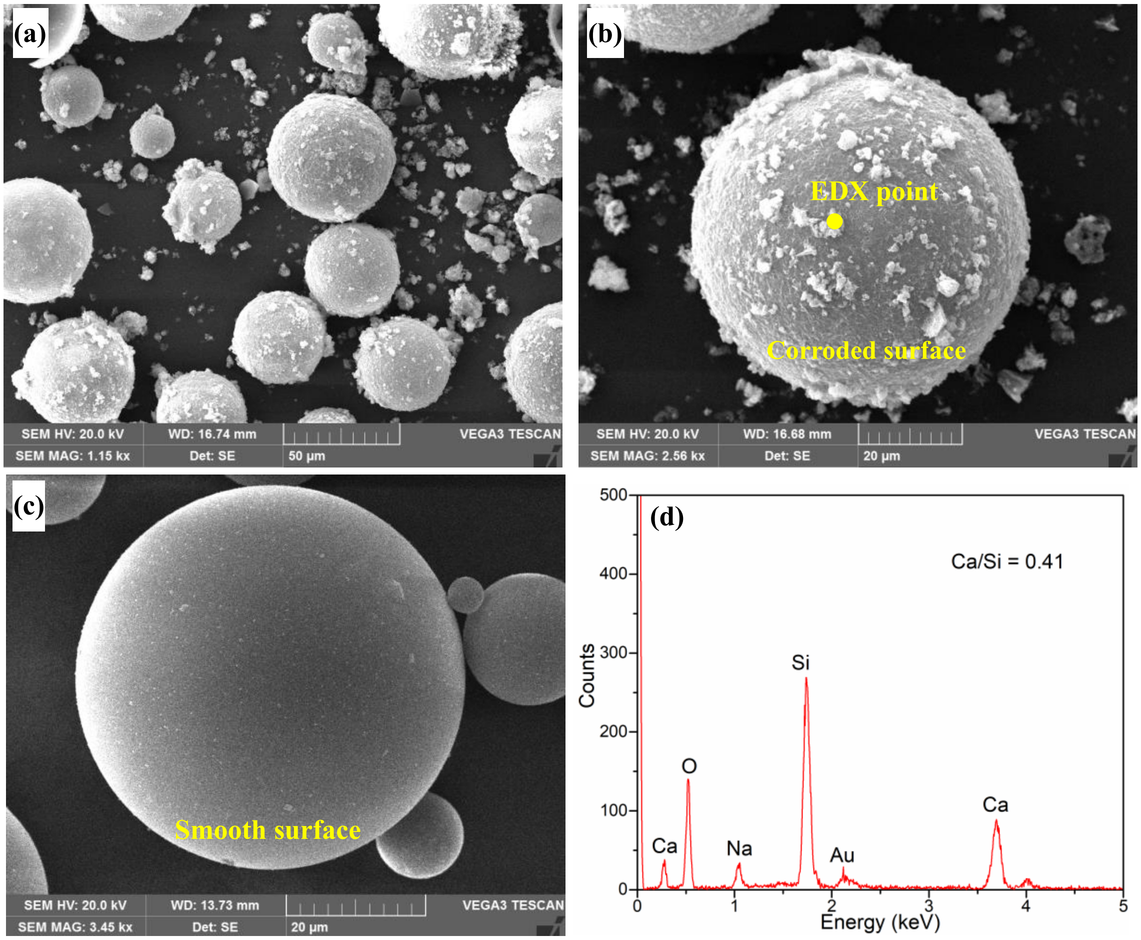

Fig. 7. Morphologies of HGM exposed to saturated $Ca(OH)_2$ solution for 28 days, (a) and b) reacted HGM particles; (c) raw HGM particles; (d) EDX of point in (b).

3.2 Functional and fundamental properties

3.2.1 Density and strength

Fig. 8a shows the density of the air-dried samples after steam curing and normal curing conditions.

The density decreased significantly with increasing content of HGM regardless of curing conditions. When 10% cement was replaced by the HGM by volume, the reduction of the density was not considerable (only 4.5%). However, nearly 15% drop in the density was found when the HGM was used in lieu of 30% cement. The density of the samples was further reduced to around 1,800 kg/m^3 when 50% cement was substituted by HGM. Since the pozzolanic reactivity and the compositions of GP were similar to HGM, the GP was thus fully replaced by HGM to further reduce the density of the UHP-LCCs. As seen, a large reduction (34%) in the density was attained to around 1600 kg/m^3. These results reveal that the incorporation of HGM as a lightweight material in the UHPC matrix was effective in reducing the density. The reason is assigned to its ultra-lightweight hollow structure.

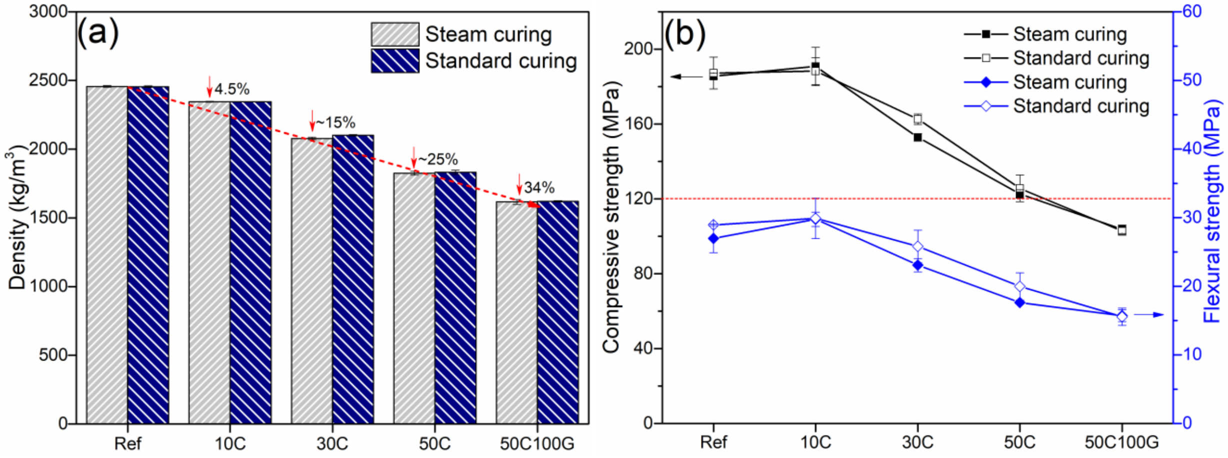

Fig. 8. Physical properties of samples, (a) Air-dried density; (b) Mechanical properties.

The mechanical properties of the samples prepared with HGM are shown in Fig. 8b. As seen, the curing condition did not have significant effects on the mechanical properties, which means that the production of high strength samples without steam curing was practical. For the reference UHPC, the compressive strength and the flexural strength could be higher than 186 MPa and 27 MPa, respectively. It is interesting to find that the replacement of 10% cement by HGM could slightly increase the mechanical properties, although the density of the sample was reduced. One point should be noted is that the use of HGM rendered a lower water demand for providing the same flowability of the mixtures. Hence, the reduced *w*/*b* ratio might enhance the mechanical properties and counteract the strength loss due to the inclusion of HGM. However, when higher amounts of cement (30% and 50%) were replaced by HGM, the compressive and flexural strengths decreased significantly. The hollow voids of HGM would break the continuity of the cementitious matrix and the reduced amount of cement could also reduce the amount of hydration products formed. Irrespectively, compressive strength of >120 MPa and flexural strength of >18 MPa could be obtained for the 50C mixture with a density of around 1,800 kg/m^3. According to the definition of UHPC in ASTM C1856C [37], the 30C (>150 MPa) and 50C could be qualified as UHPC mixtures (the compressive strength of at least 120 MPa). At the same time, the density of 50C was less than 1,920 kg/m^3, which is the upper limit of structural lightweight concrete in ACI 213R [38]. Hence, from the strength and density perspectives, the 50C mixture can be regarded as an ultra high performance lightweight cementitious composite (UHP-LCC) or lightweight UHPC. When the HGM was fully used to substitute the GP, the reductions in compressive and flexural strengths were not large. A compressive strength higher than 100 MPa could still be achieved, but the density was reduced significantly to about 1600 kg/m^3. The 50C100G is thus classified as a lightweight high performance cementitious composite (L-HPC). The similar pozzolanic reactivity and compositions of the HGM and the GP might minimize the strength loss.

3.2.2 Thermal conductivity

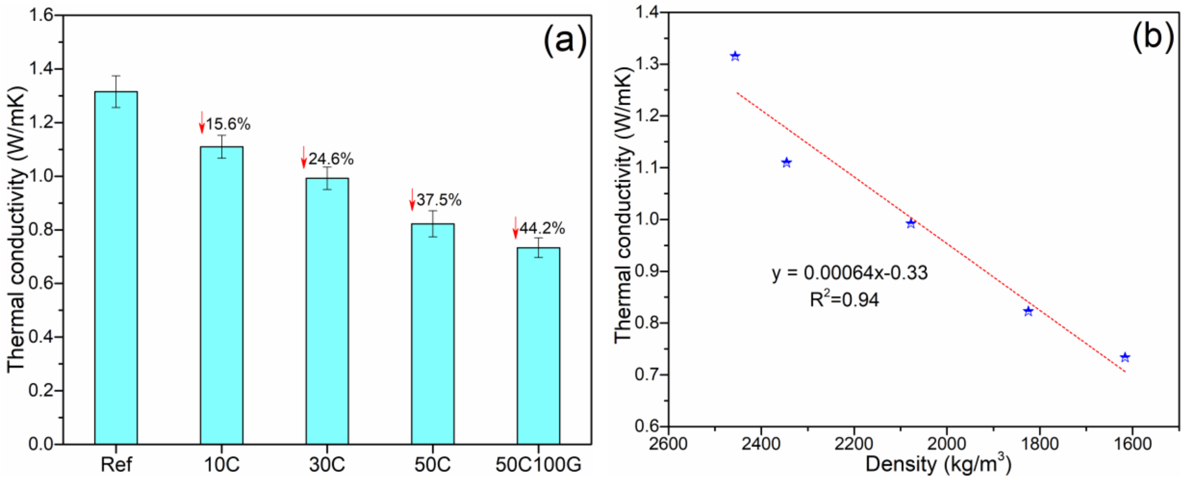

Fig. 9. Thermal conductivity of samples, (a) Thermal conductivity; (b) Relation between the density and the thermal conductivity.

The influences of using HGM on the thermal conductivity of samples are presented in Fig. 9. The thermal conductivity decreased considerably with increasing contents of HGM. For the reference UHPC, its thermal conductivity was approximate 1.3 W/mK, which is much lower than that of conventional concrete and UHPC (about 2 W/mK [56, 57]). One explanation is that the presence of glass material (i.e. GP) in the mixture was able to reduce the thermal conductivity of concrete owing to its inherent low thermal conductivity [58]. With using the HGM to replace the cement, the thermal conductivity of the UHP-LCCs decreased obviously. The hollow structure of the HGM impeded the conduction of heat in the matrix as air in the HGM has an extremely low thermal conductivity (0.026 W/mK). Hence, in the case of 50C sample, the thermal conductivity was significantly reduced by 37.5% in comparison with that of the reference sample. When HGM was used to further replace GP, the thermal conductivity of the L-HPCs was brought down further to 0.73 W/mK. Fig. 9b shows the relationship between the density and the thermal conductivity for the UHP-LCCs. As seen, the thermal conductivity linearly decreased with the decrease of density.

3.2.3 Acoustic properties

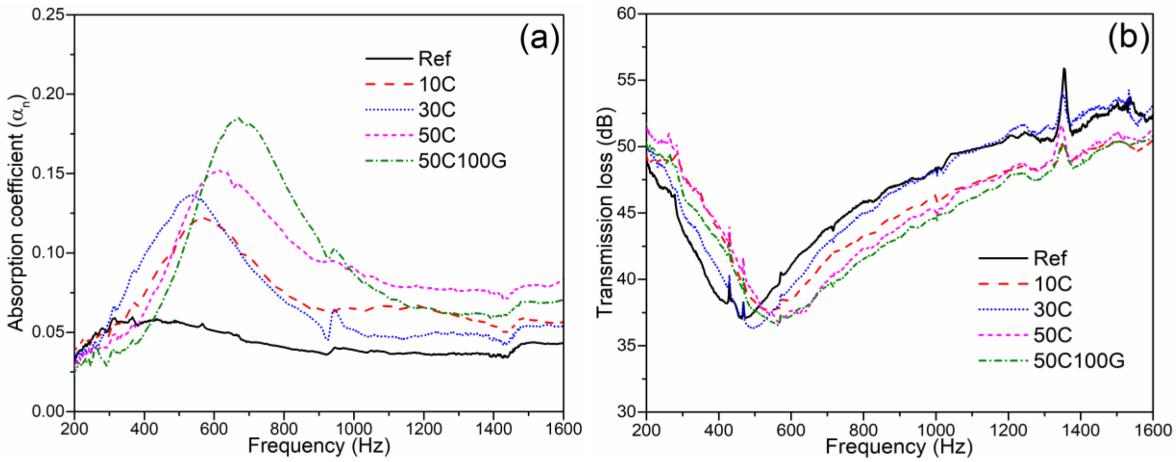

Fig. 10. Acoustic properties of samples, (a) Absorption spectra of sound; (b) Transmission loss of sound.

The acoustic properties of samples, including sound absorption and transmission loss, are shown in Fig. 10. It can be seen in Fig. 10a that the use of HGM had a huge influence on the sound absorption of UHP-LCCs and L-HPCs in the frequency range of 200-1600 Hz. The control UHPC without HGM incorporation had low absorption coefficient, while the samples prepared with HGM had much higher absorption coefficients, which means that the use of HGM in the UHP-LCCs and L-HPCs resulted in an increase of sound absorption. A closer examination of the absorption spectra reveals a small hump of sound absorption at low frequency for the reference sample, but towering peaks of sound absorption at a relatively higher frequency for the HGM-containing samples. These results indicate that the UHP-LCCs and L-HPCs incorporated with HGM were able to absorb sound, particularly at frequency of 500-800 Hz. The reason for this behavior is that the small acoustical cavities were formed on the truncation surface of the UHP-LCCs and L-HPCs when the HGM was incorporated into the mixture. Significant sound energy would be lost due to the presence of these cavities, especially at higher frequencies. That is the reason why the peak of the absorption spectra shifted to higher frequencies and higher absorption coefficients with the increase of HGM content.

For the sound transmission loss values in Fig. 10b, the UHP-LCCs and L-HPCs incorporated with HGM seemed to have a similar sound insulation property to the reference UHPC, and both had large sound transmission losses, which were higher than 35 dB. The reference UHPC had a high density and dense matrix, so that sound was difficult to penetrate the sample. Although the UHP-LCCs and L-HPCs containing HGM had a lower density and large quantity of voids inside, the sound insulation was not weakened significantly. This is because the HGM/voids located in the matrix uniformly and individually, which did not form channels for sound transmission. Moreover, the sound could be obstructed by the denser solid paste in the UHP-LCCs and L-HPCs.

3.2.4 Electrical impedance

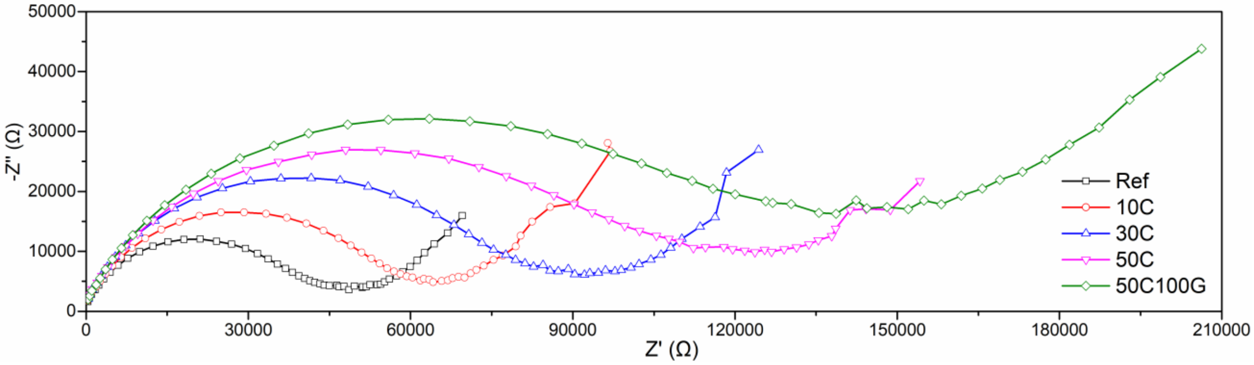

Fig. 11. Nyquist curves in impedance spectrum of samples.

The electrochemical impedance spectroscopies of the reference UHPC, UHP-LCCs and L-HPCs are depicted in Fig. 11. It can be observed that the bulk electrical resistances (R_b) of the reference UHPC and UHP-LCCs/L-HPCs were very high and the latter had a larger R_b than the former. The calculated resistivities (E_r) of the samples were 2.0×10^4, 2.6×10^4, 3.7×10^4, 4.5×10^4, 5.5×10^4 Ω·m, corresponding to Ref, 10C, 30C, 50C and 50C100G, respectively. Generally, the E_r of conventional cement concrete falls in the range of 20-100 Ω·m [59]. However, the E_r of the reference UHPC in this study could reach more than 200 times of that of the conventional concrete.

It is well known that the electrical resistance of concrete is related to the conductivity of the pore solution, types and amount of hydration products formed, connectivity of the pore structure and the porosity. On one hand, the electric conductivity of the UHPC was largely rely on the solid matrix due to the lack of pore solution, and the conductivities of the solid phases (hydration products, unhydrated cement and the SCMs) were much lower than that of pore solution. Therefore, the highly dense matrix (little porosity) and the lack of moisture in the UHPC contributed to the ultra-high electrical resistance. Hope et al. [60] also verified that the resistivity of concrete increased with the reductions in the *w*/*b* ratio and moisture. On the other hand, the presence of GP in the UHPC was expected to increase the electrical resistance due to its insulating property compared with the cement hydrates and cement particles. Such behavior was also reported in conventional GP blended concrete [61].

With the replacement of cement by HGM, the bulk/electrode arcs were amplified and the corresponding R_b was increased considerably, and the resistivities of UHP-LCCs and L-HPCs were also higher than the reference sample. The inclusion of the HGM with hollow structure was responsible for the increased R_b and E_r. Both the shell of HGM (glass) and the air in the HGM were non-conducting, resulting in an increase of electrical impedance. As the HGM was full of air, the use of HGM in lieu of solid GP could further increase the R_b and E_r of the L-HPCs. Furthermore, the finer particle size of HGM in comparison with the GP means that more hollow particles dispersed in the matrix were involved to hindering the electric conduction. Hence, the R_b and E_r were increased with the increasing HGM content in the UHP-LCCs/L-HPCs.

In general, higher E_r contributes to better concrete durability since it represents the ability of the concrete resist the migration of aggressive agents [62], especially in relation to steel corrosion [63]. The E_r in excess of 200 Ω·m is considered as negligible risk of corrosion because the high resistivity of the matrix could impede the movements of ions (such as Fe^{2+} and OH^-) in the interface of steel [64]. In this study, the UHP-LCCs and L-HPCs had ultra high E_r although they contained a large quantity of pores. That is because the individual isolated pores associated with the HGM were enclosed voids without the presence of water and compactly confined by the dense paste, which cannot facilitate current conduction. On the basic of this result, it is speculated that the HGM present in the UHP-LCCs and L-HPCs would not become a pathway for the penetration of harmful agents.

3.2.5 Water sorptivity

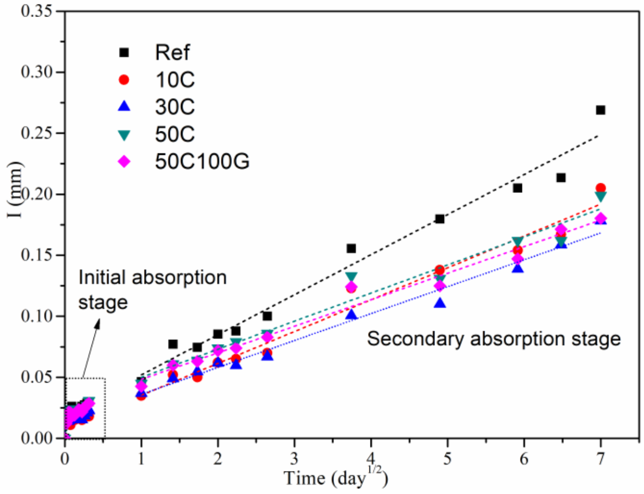

Fig. 12. Water sorptivity of samples.

The water sorptivity of unsaturated concrete is regarded as an indicator of its ability to absorb and transmit water, which is directly related to durability [65, 66]. The water sorptivity of the samples was plotted against the square root of time ($\sqrt{\text{day}}$), and the results are shown in Fig. 12. It can be seen that the progress of the water sorptivity was divide into two stages: 1) initial absorption stage (0-6 h) and 2) secondary absorption stage (＞1d). In the first stage, the water uptake of the samples was fast, but the value was low. Thus, no obvious difference among the different samples was found. During the second period, the water absorption followed a linear relationship with the square root of time. However, it is encouraging to note that the water absorption values of the samples prepared with the HGM were lower than those of the reference sample. Based on the least-square linear regression method (R^2＞0.96), the rate of water absorption in the secondary stage could be obtained [54]. The calculated rates of water penetration were 3.3×10^{-2}, 2.6×10^{-2}, 2.2×10^{-2}, 2.7×10^{-2}, 2.2×10^{-2} mm/day$^{1/2}$, corresponding to Ref, 10C, 30C, 50C, and 50C100G samples, respectively. Therefore, it is concluded that the rates of water penetration of the UHP-LCCs and L-HPCs samples were lower than that of the reference sample. These results seemed to be contrary to the percept that porous concrete is vulnerable to infiltration of deleterious substances. In unsaturated concrete, the rate of water penetration is largely governed by the absorption of the capillary pores [65, 67], whose sizes mainly locate in the range of 10 nm-5 μm [68]. That is to say, the water ingress to the samples was dominated by the capillary suction of the paste matrix rather than the voids of the HGM, because the particle size of the HGM were mostly larger than 10 μm (see Fig. 2). Three factors might account for the reduced water sorptivity: (i) as indicated in the mix proportion (Table 3), with the use of HGM, the water requirement was reduced, which would render the paste matrix denser; (ii) the voids induced by the HGM was individually isolated, and these unconnected voids could not become a channel for water ingress; (iii) the pozzolanic reactivity of the HGM facilitated the interaction between the shell of HGM and the paste (as mentioned in Section 3.1.2), which was able to form a barrier against water penetration (to be discussed in Section 3.3.2). Therefore, the influence of varying HGM contents on the rate of water absorption of the samples was not significant.

3.3 Microstructure analyses

3.3.1 Mineralogical characteristics

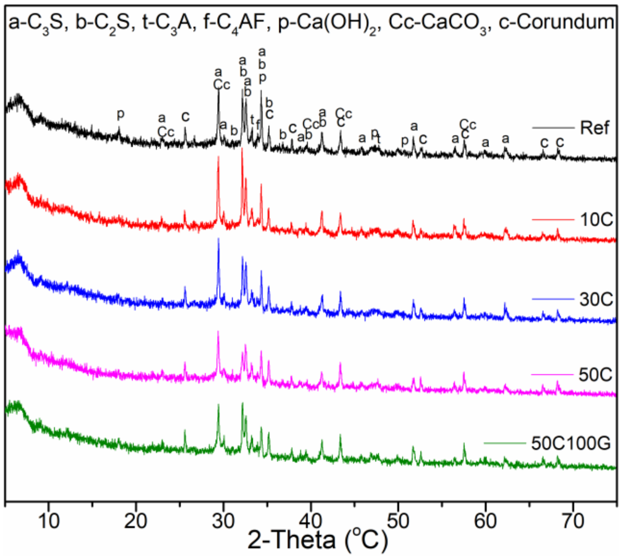

Fig. 13. XRD patterns of samples.

The XRD patterns and Q-XRD results are shown in Fig. 13 and Table 4, respectively. Plenty of unhydrated clinker phases were still identified in the samples, especially in the reference UHPC and the 10C, which means that there were a lot of cement particles only acted as fillers in the systems. Thus, replacing part of unreacted cement by HGM seemed to be practical. When the replacement level of HGM was increased, the intensities of the clinker phases were weakened due to the reduced amount of cement. Meanwhile, with the increase of HGM content, the signal peak of portlandite (CH, PDF# 44-1481) disappeared. This is consistent with the Q-XRD analyses. Since both the GP and the HGM were glass materials with amorphous structures, the substitution of GP with HGM did not affect the XRD diffractograms.

From Table 4, it is found that the amounts of unreacted clinker phases in 10C and 30C were comparable or even higher than those of the reference sample. This seems to be contrary to the fact that reduced amounts of cement content were present in the HGM incorporated samples. The behavior might be due to the partial replacement of cement by HGM required a less amount of water to maintain the similar workability (see Table 3) and as a result, more clinker phases remained unhydrated. With the further increase in the replacement level of HGM, smaller quantities of unreacted clinker phases were detected by Q-XRD. On the other hand, the amorphous content was increased due to the higher amounts of HGM (glass material) and the formation of secondary C-S-H from HGM (to be discussed in Section 3.3.2). When GP was replaced by the HGM, the amount of water required for mixing was further reduced so that the unhydrated clinker phase contents were increased slightly. Meanwhile, the amorphous material content decreased because the solid glass particles (GP) were replaced by the hollow glass particles (HGM).

Table 4 Crystalline phases in the samples by Q-XRD.

Phases (%)	Ref	10C	30C	50C	50C100G
C_3S	16.2	18.8	16.5	12.1	13.0
C_2S	13.8	17.0	13.8	9.2	10.9
C_3A	2.1	2.7	2.6	1.6	3.1
C_4AF	5.1	4.3	3.6	3.9	3.5
Calcite	8.3	9.7	9.1	7.7	7.7
CH	1.6	-	-	-	-
Amorphous	52.9	46.9	54.4	65.6	61.9

Note: ‘-’ means undetectable phases.

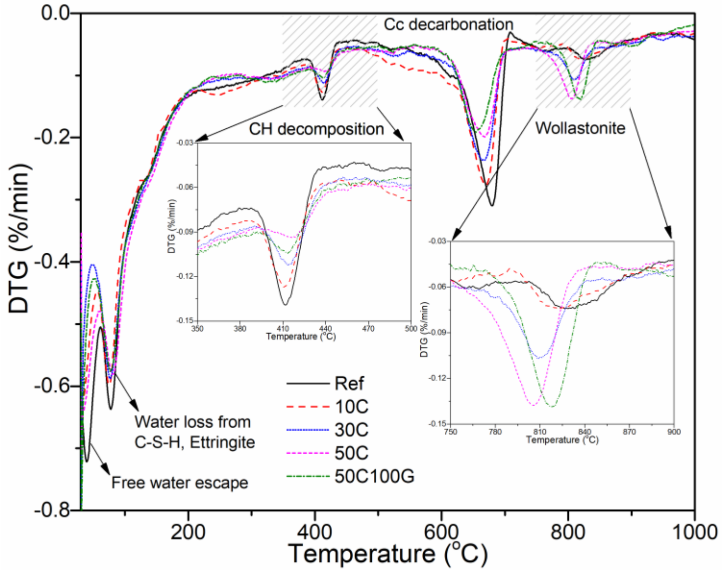

Fig. 14. DTG curves of samples.

Since the low content of CH was undetectable by XRD, TG/DTG was used for such purpose and the DTG curves are shown in Fig. 14. There were some small peaks of CH dihydroxylation [69] occurred at the temperature of 350-450 °C, validating the low content of CH in the samples. The magnification of these peaks clearly shows that the peak intensity became weaker with increased HGM contents, indicating the reduced amount of CH. This result is attributed to the lower cement content and the lower hydration degree due to less water was available in the HGM-containing mixtures. Furthermore, the pozzolanic reaction of HGM would also consume some CH as indicated in the Chapelle test. An interesting phenomenon is observed at temperature of around 830 °C. These well-defined endothermic peaks are usually ascribed to the transformation of C-S-H into wollastonite ($CaSiO_3$) [70]. The peak was intensified and shifted to the lower temperature with the increase of HGM content. This may be due to the pozzolanic reaction of the silica-rich HGM reduced the Ca/Si ratio of C-S-H (see Fig. 18), which altered the kinetics of transformation. The explanation is supported by the studies of Rodriguez et al. [70] and Garbev et al. [71].

3.3.2 Morphological observation

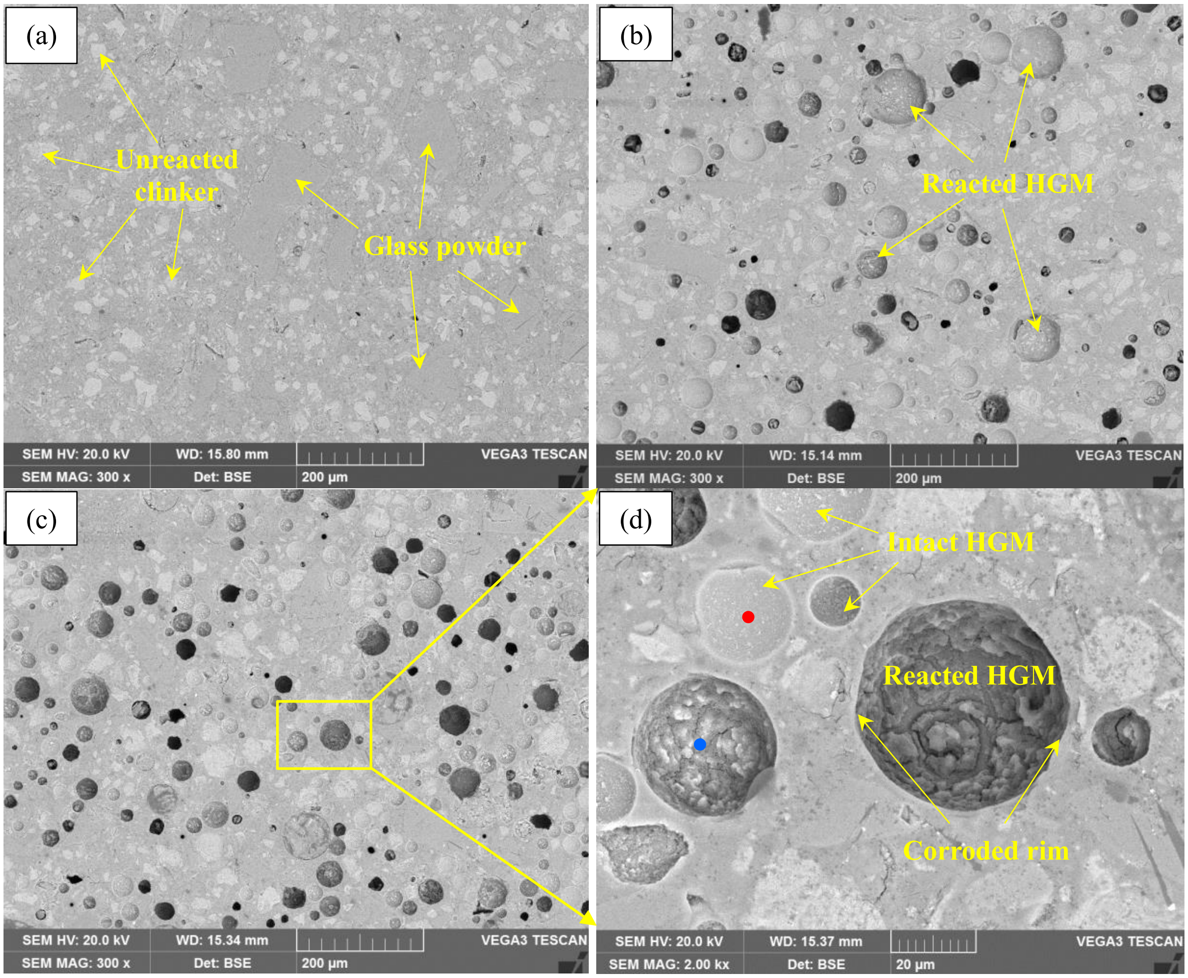

Fig. 15. BSE images of samples, (a) Ref; (b) 30C; (c) 50C; (d) Magnification of c.

Fig. 15 shows the BSE micrographs of the reference UHPC and UHP-LCCs. It can be seen in Fig. 15a that there were many unreacted clinker phases presenting in the reference sample, which is consistent with the XRD results. Also, GP particles were observed which acted as micro-aggregates in the matrix. The reference UHPC exhibited a very dense microstructure with few pores. When 30% cement was replaced by HGM (Fig. 15b), many pores (dark areas) with different sizes were found together with the unhydrated clinker minerals and GP. These cavities brought by the HGM were responsible for the lower density and better sound absorption as compared to the reference sample. Also, it is noted that the pores were isolated instead of interconnected network. For the 50C sample shown in Fig. 15c, more cavities were found due to the increased amount of HGM incorporation. It should be noticed that the paste matrix in the 50C still contained lots of unreacted clinker phases. This indicates that more than 50% cement in the UHPC served only as a filler. Thus, the strategy of 50% substitution of cement by HGM seemed to be plausible in the "cement-overdosed" UHPC system. As the HGM with smooth surface absorbed little water, the use of HGM could provide more water for the hydration of the residual cement. A closer examination on the HGM in Fig. 15d shows that the HGM particles were intact from an interior view, but some interior shells of HGM were corroded. The elemental compositions of two representative points were analyzed by EDX in Table 5. As shown, the red point in the smooth internal wall had a lower Ca/Si ratio (0.34) than the blue point in the rougher internal wall (Ca/Si=2.24). The higher Si and Na concentrations at the red point indicate this was an unreacted glass shell, while the higher Ca and Al contents at the blue point reveal the formation of C-S-H, which was the result of the pozzolanic reaction between the HGM and hydration products of cement. This is in agreement with the observations in Section 3.1.2. The reaction of the shell is expected to improve the interfacial transition zone (ITZ) between the HGM and the cementitious matrix, which contributed to the enhanced impermeability of the UHP-LCCs. Moreover, the formation of additional C-S-H on the shell of HGM would reinforce the shells/voids to bear the local stress exerting on the HGM.

Table 5 EDX analysis of points in Fig. 15d.

Element %	Red point	Blue point
O	63.6	53.2
Al	1.2	5.1
Si	24.4	12.9
Ca	8.4	28.9
Na	2.0	-
K	0.4	-
Ca/Si	0.34	2.24
Si/Al	20.33	2.53

3.3.3 Gel pores in the paste matrix

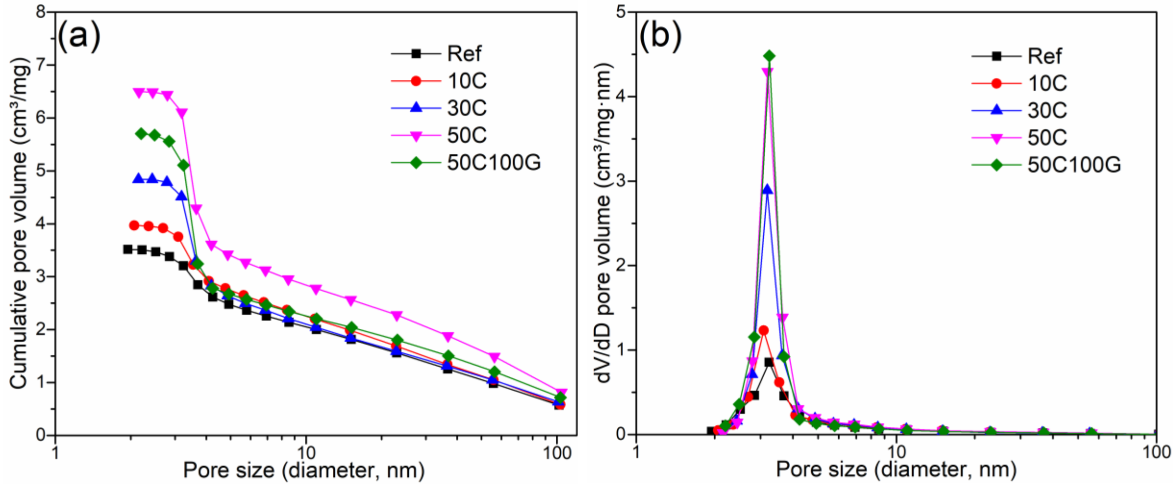

Fig. 16. Pore structure of samples determined by nitrogen adsorption method, (a) Cumulative pore volume; (b) Pore size distribution.

The BET nitrogen adsorption was determined to understand the mesopore structure of the paste matrix in the samples. The results are shown in Fig. 16. As the pores induced by the HGM (>10 μm) were outranged and cannot be detected by this method (1-300 nm), this test only focused on the gel pores and mesopores (< 100 nm) in the paste matrix of the samples. In Fig. 16a, it is noted that the cumulative pore volume increased with the increasing replacement of cement by HGM. There was a sudden increase of the total pore volume at the pore size of around 5 nm, especially in the cases containing high volume of HGM. This phenomenon can be attributed to the presence of large quantity of fine pores in the UHP-LCCs/L-HPCs, as shown in Fig. 16b. The pore size distributions indicate that most of pores were smaller than 5 nm, which belonged to the range of gel pores [72]. As seen, the incorporation of HGM increased the number of gel pores significantly. Since the gel pores are the interparticle spaces between C-S-H sheets [68], the greater volume of the gel pores seems to imply the increased formation of C-S-H. As mentioned, a lot of cement in the UHPC was unhydrated, in turn, the use of HGM in lieu of cement could form additional C-S-H. Therefore, the increasing contents of HGM in the UHP-LCCs/L-HPCs might increase the volume of gel pores. This result also verifies the active reaction between the HGM and the hydration products. When the GP was replaced by the same volume of HGM, their similar reactivity (see Section 3.1.1) rendered them to form comparable volume of pozzolanic C-S-H and gel pores.

4 Discussion

4.1 **Strategies for preparing ultra high-performance lightweight composites**

One advantage of lightweight concrete is to reduce the dead load of structural elements. The specific strength (strength/density) is usually used to represent the material efficiency of the lightweight concrete. Fig. 17 shows the comparison of specific strength between the samples in this study and high strength/performance lightweight concrete in other works with density values between 1,500-2,100 kg/m^3 [5, 6, 8, 10, 12, 16, 73-89]. It can be seen that the specific strengths of the developed UHP-LCCs and L-HPCs in this study exceeded 60kPa/kg/m^{-3} regardless of curing conditions (detailed data are shown in Table 6), which were higher than those reported in previous works of high strength/performance lightweight concrete (mainly ranging in 20-50kPa/kg/m^{-3}). This excellent behavior of UHP-LCCs was mainly dependent on three characteristics: paste matrix, lightweight material and their bonding condition. Based on these characteristics and the high specific strength of the UHP-LCCs, several strategies to prepare ultra high-performance lightweight composites are proposed.

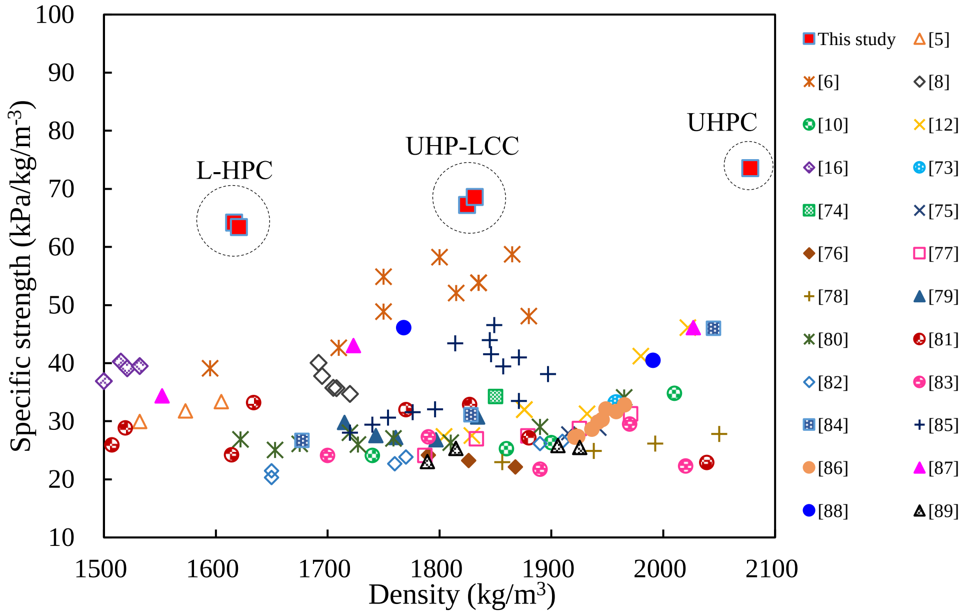

Fig. 17. Comparison of specific strength between UHP-LCCs/L-HPCs and other high-performance lightweight concrete.

(1) Use of UHPC system

In order to develop the ultra high-performance lightweight composites, UHPC would need to be used as cementitious matrix due to its excellent mechanical properties and superior durability. The advancement of UHPC is attributed to the optimum packing of powders and the use of a low *w*/*b* ratio, which contribute to a dense microstructure with low porosity. Therefore, it was evident that the use of UHPC system could provide a strong matrix for the UHP-LCCs. As indicated by previous studies [7], the durability of lightweight concrete was primarily governed by the quality of the cement paste although the concrete contained porous aggregates. In the UHP-LCCs, the UHPC paste was responsible for binding the lightweight particles, providing the strength and resisting against the infiltration of deleterious substances. It is known that the lower mechanical properties and higher brittleness of the conventional lightweight concrete usually restrict its wide applications. The addition of fibers was proven to be an effective means to improve the tensile strength and toughness of the lightweight concrete [8, 9]. In this study, the utilization of UHPC system incorporating with steel fiber could strengthen the flexural toughness and mitigate the brittleness risk via crack bridging effect of fiber. Thus, the UHP-LCCs could obtain a higher flexural strength.

(2) Optimized selection of lightweight media

For lightweight aggregate concrete, the type of aggregate plays an important role in controlling the mechanical properties because the lightweight aggregate with a high porosity is the weakest component in the concrete [6]. However, most high strength lightweight aggregates normally have a dried density higher than 800 kg/m^3, which makes them difficult to prepare very low-density lightweight concrete. Thus, in this study, the HGM with a hollow structure was employed as the lightweight media in the production of the UHP-LCCs. The advantages of HGM are as follows: (i) high isostatic compression strength (stiff shell) and low apparent density (420 kg/m^3); (ii) low water absorption due to the vitreous structure and smooth surface; (iii) spherical shapes and small particle size; (iv) pozzolanic reactivity (siliceous source). On the basic of above, the use of the HGM in the UHPC system could mitigate the strength loss as low as possible caused by the incorporation of hollow particles. In addition, due to the very low density of HGM, the density of the UHP-LCCs could be reduced. The low water absorption (closed pores) and the spherical shape of HGM were beneficial to reducing the water demand and improving the workability of the UHP-LCCs, which facilitated the compaction of the paste matrix and improve the homogeneity of HGM.

(3) Improvement of ITZ by hydrothermal curing

The ITZ is a primary component contributing to the mechanical properties and durability, especially for high strength concrete. As the UHP-LCCs was consisted of a high-performance paste and a lightweight material, the ITZ quality between them was also vital for the properties of UHP-LCCs. In particular, the smooth surface of HGM was not conducive to producing a good paste-HGM sphere interface. In this study, steam curing was adopted to accelerate the glass dissolution and pozzolanic reaction of the HGM. It was found that the shell of the lightweight HGM actively reacted with the cementitious paste to form new hydration products. Although the curing time was short, the reactivity of the HGM could be effectively activated in the hydrothermal curing process. The reaction improved the bonding between the paste and the lightweight media, so that the reacted HGM shell might in turn become an effective barrier to sustain local stresses and prevent forming microcracks in the ITZ. Such phenomenon was also confirmed by a recent study [90], which found that the hydrothermal curing was beneficial to refining the pores and improving the interface between the HGM and the paste matrix. Besides, this study reported that the UHP-LCCs cured under standard curing for a prolonged time could also attain similar mechanical properties to those cured under steam curing. Therefore, the curing at ambient temperature was also practical to produce this lightweight UHPC.

4.2 Synergistic effects of UHPC and HGM

It is interesting to note that the small volume of HGM incorporation in the UHPC matrix slightly increase the mechanical properties and specific strength regardless of curing conditions (see Fig. 8 and Table 6). Similar trends were also observed by other studies especially at lower substitution ratio of HGM [91-93]. Although the incorporation of HGM increased the amount of voids in the matrix, several benefits were also triggered by the HGM inclusion: The use of a small amount of HGM could reduce the entrapped air content of the paste matrix owing to the lubrication effect [91]. The HGM also improved the workability thanks to its smooth surface and spherical shape [94]. Hence, the water demand for the mixture could be reduced to maintain a similar flow value (see Table 3). This was beneficial to enhance the strength of UHPC matrix and counteract the loss of strength induced by the voids of HGM. Another study [95] also showed that the enhancements of mechanical properties were attained with reducing the water to cement ratio in the presence of HGM. The interaction between the HGM and the alkaline hydrates facilitated the bonding of HGM and the paste matrix (as shown in Fig. 15). As reported in Ref. [91], the HGM particles with a thin shell thickness might be broken when subjected to loading. The additional C-S-H formation on the surface of the HGM due to the pozzolanic interaction would reinforce the thin shell, which helped to resist the percolation of cracks across the interface. The textural changes of HGM under hydrothermal curing had been pointed out to drastically increase the load bearing capacity of the matrix [90]. Therefore, the HGM in this study acted not only as a lightweight filler, but also as a SCM. The dual effects are similar to what have been achieved in the cementitious mixtures prepared with fly ash cenospheres [91], and the reaction of fly ash cenospheres in the cement matrix might be the main reason for obtaining higher strength even with a lower density [96].

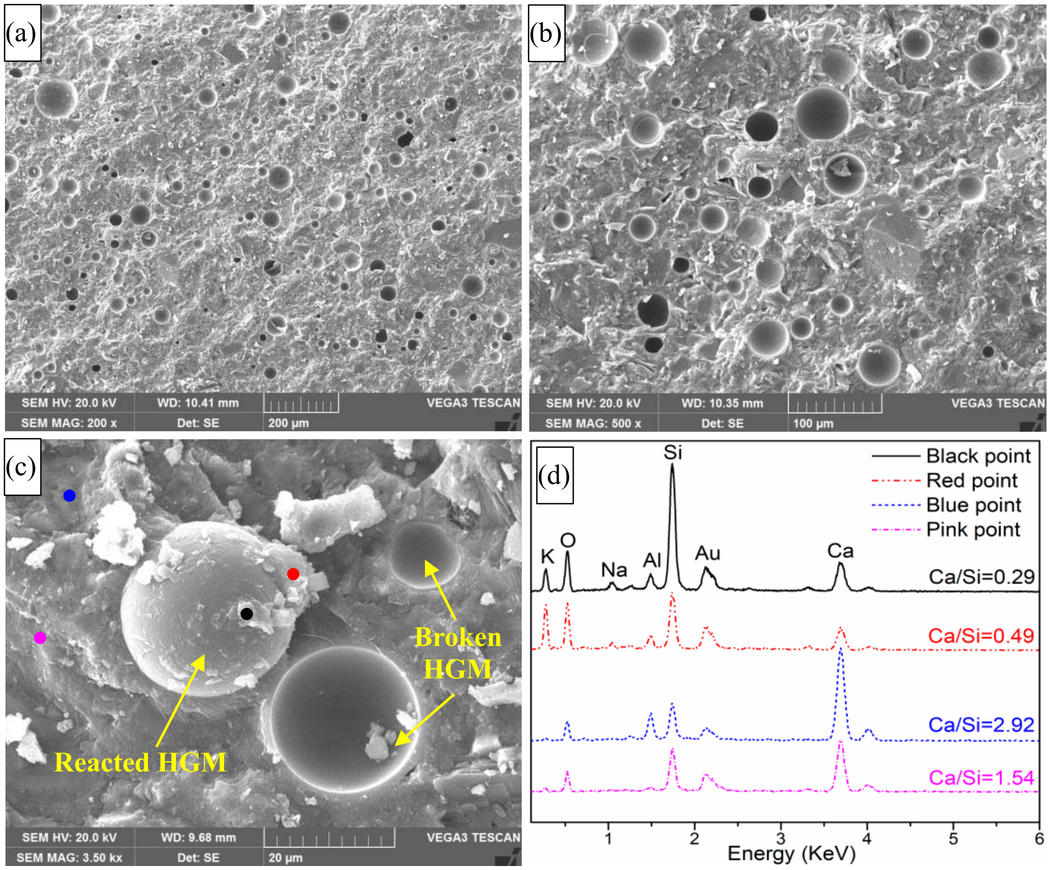

Fig. 18. SEM images of 10C, (a, b) Fractured morphologies; (c) Damage mode of HGM; (d) Spectrums of EDX points in (c).

This is especially evident for the samples subjected to hydrothermal curing. The fractured surfaces of the samples shown in Figs. 18a and 18b demonstrate most of the damages occurred across the glass shells instead of the interfacial bonds. This phenomenon qualitatively revealed a higher interfacial strength owing to the physicochemical interaction of HGM with the paste matrix. Fig. 18c presents the two failure modes of HGM, one was break through the particle shell, and the other one was damage along the sphere surface. Furthermore, it is noticed that the surface of HGM was rough and some additional products were attached on the surface. This implies some surface reaction of HGM on its shell. Further analysis by EDX in Fig. 18d shows that the surface products had a lower Ca/Si ratio than the hydrates surrounding because the HGM was rich in SiO_2. This behavior is consistent with the results of Section 3.1. The formation of the low Ca/Si C-S-H would strengthen the interface between the HGM and the matrix. Overall, the above contributions surpassed the negative effects of the voids in HGM on the strength when it was incorporated in the UHPC at a low volume.

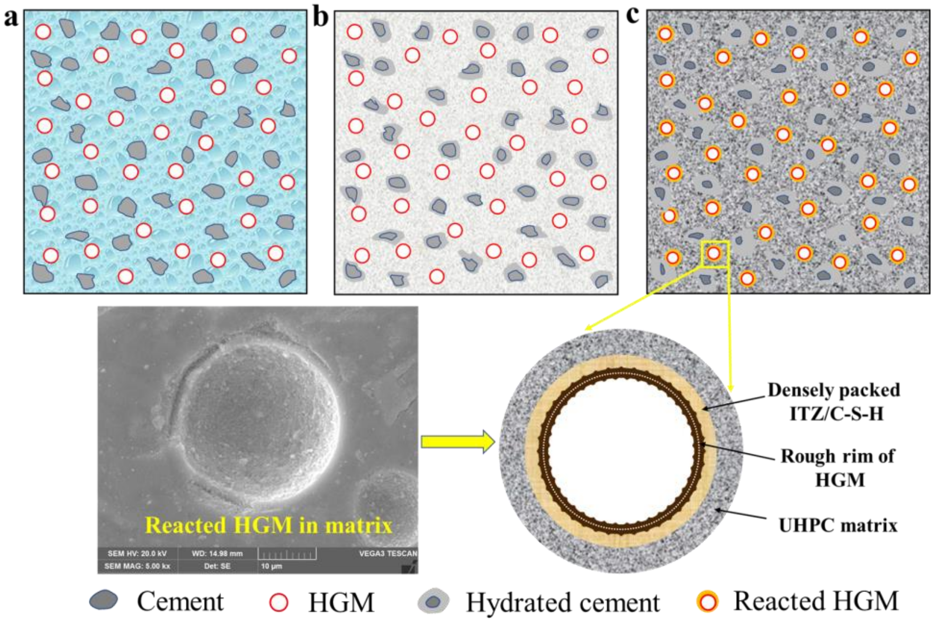

Fig. 19. Schematic of UHP-LCCs prepared with HGM, (a) Fresh state; (b) Hardened state; (c) Mature state.

The combined use of the UHPC and the HGM was effective to prepare a high-performance lightweight composite with ultra high strength and low density. The functional and durability properties of the UHP-LCCs were improved as shown in Table 6. These benefits were derived from the synergistic effects of the UHPC and the HGM in three stages, as shown in Fig. 19: (i) in the fresh state, to achieve a similar fluidity, the incorporation of HGM allowed to lower the water demand of the mixture (see Table 3) because of its spherical shape and smooth surface, which improved the workability of matrix [97]. This is particularly important for the UHPC system since a low *w*/*b* ratio and good homogeneity are imperative factors to attain high strength. The reduced *w*/*b* ratio implied a higher strength of paste matrix, which could partly compensate the loss strength due to the degrading effect of HGM. (ii) in the hardened stage, the cement hydrated formed a dense

UHPC paste, which was the main skeleton for achieving high strength. The fine and hollow HGM particles were packed tightly in the UHPC matrix to reduce the density (as shown in Fig. 19). The coupled use of this hollow lightweight material was conducive to improving the thermal insulation and sound absorption (see Figs. 9 and 10). As compared to the thermal conductivity of conventional UHPC and cement mortar (2.1-2.5 W/mK [57, 84]), the reduction in the thermal conductivity of the UHP-LCCs (50C: 0.82 W/mK) was significant (＞60%). (iii) in the mature state of the UHP-LCCs, the degree of cement hydration was further increased, and a highly dense paste was formed. The pozzolanic reaction of the HGM with the hydration products was able to improve the ITZ between the HGM and the paste matrix. Fractured morphology in Fig. 18 validates the intensified ITZ because the failure across the sphere was the major damage mode of HGM instead of failure along the interface. Hence, the voids of HGM could be tightly confined by the additional low Ca/Si C-S-H on the shell of HGM. As a result, the resistances of the UHP-LCCs to electrical conduction and water ingress were enhanced (Figs. 11 and 12).

Table 6 Physical, mechanical and functional properties of samples.

Mix	Air-dried density (kg/m^3)		Compressive strength (MPa)		Flexural strength (MPa)		Thermal conductivity (W/mK)	Rate of water absorption (mm/day$^{1/2}$)	Electrical resistivity (Ω·m)	Specific strength (kPa/kg/m^{-3})	
	SC	WC	SC	WC	SC	WC	SC	SC	SC	SC	WC
Ref	2456	2455	185.6	187.2	27.0	28.9	1.32	3.3×10^{-2}	2.0×10^{4}	75.6	76.3
10C	2345	2345	190.8	188.3	29.8	29.9	1.11	2.6×10^{-2}	2.6×10^{4}	81.3	80.3
30C	2078	2101	152.9	162.6	23.1	25.8	0.99	2.2×10^{-2}	3.7×10^{4}	73.6	77.4
50C	1825	1832	122.6	125.6	17.6	20.0	0.82	2.7×10^{-2}	4.5×10^{4}	67.2	68.6
50C100G	1616	1621	103.8	102.8	15.7	15.6	0.73	2.2×10^{-2}	5.5×10^{4}	64.2	63.4

Note: SC means steam curing for 2 days, WC represents water curing for 112 days.

5 Conclusion and future prospects

In this study, the development of an ultra high-performance lightweight cementitious composite (UHP-LCC) was investigated by the combined use of an ultra high-performance binder (i.e. UHPC) and micro-sized voids with a high strength shell (i.e. HGM). The following conclusions from the experimental investigation can be drawn:

(1) The HGM selected as lightweight media had a non-crystalline structure, spherical shape and smooth surface, which was effective in reducing the water demand and improving the workability. Due to its ultra-lightweight hollow structure, the overall densities of the

UHP-LCCs were reduced significantly.

(2) When 50% cement was substituted by HGM, the density of the UHP-LCCs dropped to 1,825 kg/m^3, but an ultra high compressive strength of 123 MPa could still be achieved. Further replacing the GP by the HGM, a lightweight HPC (L-HPC) with compressive strength of higher than 100 MPa and a density of about 1,600 kg/m^3 was attained. The high quality of UHPC paste, high performance micro-sized voids with a high stiff shell, and intensified ITZ were responsible for the ultra high strength and the low density. The curing conditions did not have significant effects on the mechanical properties of samples.

(3) The incorporation of HGM was effective in reducing the thermal conductivity of the UHP-LCCs. The use of HGM in the UHP-LCCs and the L-HPCs significantly improved the sound absorption due to the presence of large quantities of acoustical cavities.

(4) The electrical resistance of the UHP-LCCs and L-HPCs was much higher than that of reference UHPC, and was significantly increased with the increase of HGM content. Moreover, the rates of water absorption of the UHP-LCCs and L-HPCs were lower than that of the reference UHPC. Therefore, the pores brought by the HGM did not facilitate electrical conduction and water ingress. The enhanced paste quality, isolation of the HGM and the improved interface of the HGM contributed to the highly impermeable property of the UHP-LCCs.

(5) The specific strengths of the developed UHP-LCCs and L-HPCs were higher than those of current high strength/performance lightweight concrete. The combined use of UHPC and HGM was feasible to prepare the UHP-LCCs and L-HPCs with ultra high strength and low density (high structural efficiency). The use of UHPC system, optimized selection of lightweight material and improvement of ITZ were effective strategies to produce the UHP-LCCs with good performance.

This study innovatively demonstrated that, by introducing micro-sized voids with a high strength shell, an UHP-LCC could be produced. Encouragingly, the developed UHP-LCC containing a large quantity of voids had comparable or even superior durability properties than conventional UHPC. Therefore, the results of this study provide a new approach for designing and producing a lightweight UHPC. Fine aggregates, such as lightweight aggregates, can be incorporated to further improve the properties of the UHP-LCCs and reduce the consumptions of cementitious materials. This kind of UHP-LCCs would be a promising solution for practical engineering applications, such as long-span platforms. In addition, it is of great importance to produce a more cost-effective and environmentally friendly HGM with a view to promoting the sustainable development of UHP-LCCs.

Acknowledgement

The authors gratefully acknowledge the financial support of The Hong Kong Polytechnic University. The technical assistances of Ms. Dorothy Chan and Ms. Emily Fung (Technicians in the Department of Civil and Environmental Engineering) in carrying out the BET and acoustic properties tests are gratefully acknowledged. Thanks are also due to Dr. Zhang Yangyang for his assistance in the Q-XRD analysis. We express our appreciation to the editor and all the anonymous reviewers for their valuable comments for the improvement of this work.

References

[1] T.W. Bremner, T.A. Holm, High performance lightweight concrete-A review, ACI Material Journal, SP 154-1 (1995) 1-19.
[2] T.A. Holm, J.P. Ries, Benefits of lightweight HPC, HPC Bridge Views, 17 (2001) 3.
[3] M.-H. Zhang, X. Liu, K.-S. Chia, High-strength high-performance lightweight concrete: A review, In Proceedings of the 9th International Symposium on High Performance Concrete, New Zealand Concrete Society, Rotorua, New Zealand, (2011).
[4] H. S. Wilson, V.M. Malhotra, Development of high strength lightweight concrete for structural applications, International Journal of Cement Composites & Lightwght Concrete, 10 (1988) 79-90.
[5] J.A. Rossignolo, M.V.C. Agnesini, J.A. Morais, Properties of high-performance LWAC for precast structures with brazilian lightweight aggregates, Cement & Concrete Composites, 25 (2003) 77-82.
[6] M.-H. Zhang, O.E. Gjørv, Mechanical properties of high-strength lightweight concrete, ACI Material Journal, 88 (1991) 240-247.
[7] M.-H. Zhang, O.E. Gjørv, Permeability of high-strength lightweight concrete, ACI Material Journal, 88 (1991) 463-469.
[8] S. Iqbal, A. Ali, K. Holschemacher, T.A. Bier, Mechanical properties of steel fiber reinforced high strength lightweight self-compacting concrete (SHLSCC), Construction and Building Materials, 98 (2015) 325-333.
[9] J. Li, J. Niu, C. Wan, X. Liu, Z. Jin, Comparison of flexural property between high performance polypropylene fiber reinforced lightweight aggregate concrete and steel fiber reinforced lightweight aggregate concrete, Construction and Building Materials, 157 (2017) 729-736.
[10] X. Liu, K.S. Chia, M.-H. Zhang, Water absorption, permeability, and resistance to chloride-ion penetration of lightweight aggregate concrete, Construction and Building Materials, 25 (2011) 335-343.
[11] M. Lopez, L.F. Kahn, K.E. Kurtis, Effect of internally stored water on creep of high-performance concrete, ACI Materials Journal, 105 (2008) 265-273.
[12] M.-H. Zhang, L. Li, P. Paramasivam, Shrinkage of high-strength lightweight aggregate concrete exposed to dry environment, ACI Materials Journal, 102 (2005) 86-92.
[13] Arnon Bentura, Shin-ichi Igarashib, K. Kovler, Prevention of autogenous shrinkage in high-strength concrete by internal curing using wet lightweight aggregates, Cement and Concrete Research 31 (2001) 1587–1591.
[14] D. Cusson, T. Hoogeveen, Internal curing of high-performance concrete with pre-soaked fine lightweight aggregate for prevention of autogenous shrinkage cracking, Cement and Concrete Research, 38 (2008) 757-765.

[15] B. Chen, J. Liu, Contribution of hybrid fibers on the properties of the high-strength lightweight concrete having good workability, Cement and Concrete Research, 35 (2005) 913-917.

[16] B. Chen, J. Liu, Experimental application of mineral admixtures in lightweight concrete with high strength and workability, Construction and Building Materials, 22 (2008) 1108-1113.

[17] M.S. Nadesan, P. Dinakar, Influence of type of binder on high-performance sintered fly ash lightweight aggregate concrete, Construction and Building Materials, 176 (2018) 665-675.

[18] N. Atmaca, M.L. Abbas, A. Atmaca, Effects of nano-silica on the gas permeability, durability and mechanical properties of high-strength lightweight concrete, Construction and Building Materials, 147 (2017) 17-26.

[19] Christopher J. Waldron, Thomas E. Cousins, Adil J. Nassar, J.P. Gomez, Demonstration of use of high-performance lightweight concrete in bridge superstructure in Virginia, Journal of Performance of Constructed Facilities, 19 (2005) 146-154.

[20] Thomas A. Holm, T.W. Bremner, State-of-the-art report on high-strength, high-durability structural low-density concrete for applications in severe marine environments, U.S. Army Corps of Engineers, Engineer Research and Development Center, 2000.

[21] T. Cousins, C. Roberts-Wollmann, M.C. Brown, High-performance high-strength lightweight concrete for bridge girders and decks, Transportation Research Board, National Cooperative Highway Research Program (NCHRP) Report 733, Washington, D.C., (2013).

[22] T.A. Holm, J.P. Ries, Chapter 9: High-performance lightweight concrete, ESCSI's Reference Manual for the Properties and Applications of Expanded Shale, Clay and Slate Lightweight Aggregate, Expanded Shale, Clay & Slate Institute (ESCSI), (2007).

[23] X. Wang, R. Yu, Q. Song, Z. Shui, Z. Liu, S. Wu, D. Hou, Optimized design of ultra-high performance concrete (UHPC) with a high wet packing density, Cement and Concrete Research, 126 (2019) 105921.

[24] K. Wille, A.E. Naaman, G.J. Parra-Montesinos, Ultra-high performance concrete with compressive strength exceeding 150 MPa (22 ksi): A simpler way, ACI materials journal, 108 (2011).

[25] N.A. Soliman, A. Tagnit-Hamou, Using particle packing and statistical approach to optimize eco-efficient ultra-high-performance concrete, ACI Materials Journal, 114 (2017).

[26] A. Arora, A. Almujaddidi, F. Kianmofrad, B. Mobasher, N. Neithalath, Material design of economical ultra-high performance concrete (UHPC) and evaluation of their properties, Cement and Concrete Composites, 104 (2019) 103346.

[27] Q.L. Yu, P. Spiesz, H.J.H. Brouwers, Ultra-lightweight concrete: Conceptual design and performance evaluation, Cement and Concrete Composites, 61 (2015) 18-28.

[28] H. Du, Properties of ultra-lightweight cement composites with nano-silica, Construction and Building Materials, 199 (2019) 696-704.

[29] S.K. Adhikary, Ž. Rudžionis, D. Vaičiukynienė, Development of flowable ultra-lightweight concrete using expanded glass aggregate, silica aerogel, and prefabricated plastic bubbles, Journal of Building Engineering, 31 (2020) 101399.

[30] R. Yu, D.V. van Onna, P. Spiesz, Q.L. Yu, H.J.H. Brouwers, Development of Ultra-Lightweight Fibre Reinforced Concrete applying expanded waste glass, Journal of Cleaner Production, 112 (2016) 690-701.

[31] P. Sikora, T. Rucinska, D. Stephan, S.-Y. Chung, M. Abd Elrahman, Evaluating the effects of nanosilica on the material properties of lightweight and ultra-lightweight concrete using image-based approaches, Construction and Building Materials, 264 (2020) 120241.

[32] M. Valipour, K.H. Khayat, Coupled effect of shrinkage-mitigating admixtures and saturated lightweight sand on shrinkage of UHPC for overlay applications, Construction and Building Materials, 184 (2018) 320-329.

[33] W. Meng, K. Khayat, Effects of saturated lightweight sand content on key characteristics of ultra-high-performance concrete, Cement and Concrete Research, 101 (2017) 46-54.

[34] J. Liu, C. Shi, N. Farzadnia, X. Ma, Effects of pretreated fine lightweight aggregate on shrinkage and pore structure of ultra-high strength concrete, Construction and Building Materials, 204 (2019) 276-287.

[35] Y. Sun, R. Yu, Z. Shui, X. Wang, D. Qian, B. Rao, J. Huang, Y. He, Understanding the porous aggregates carrier effect on reducing autogenous shrinkage of Ultra-High Performance Concrete (UHPC) based on response surface method, Construction and Building Materials, 222 (2019) 130-141.

[36] K. Liu, R. Yu, Z. Shui, X. Li, C. Guo, B. Yu, S. Wu, Optimization of autogenous shrinkage and microstructure for Ultra-High Performance Concrete (UHPC) based on appropriate application of porous pumice, Construction and Building Materials, 214 (2019) 369-381.

[37] ASTM C1856C/1856M, Standard practice for fabricating and testing specimens of ultra-high performance concrete, American Society of Testing Materials, (2017).

[38] ACI 213R-03, Guide for structural lightweight-aggregate concrete, American Concrete Institute, (2003).

[39] J.-X. Lu, Z.-H. Duan, C.S. Poon, Combined use of waste glass powder and cullet in architectural mortar, Cement and Concrete Composites, 82 (2017) 34-44.

[40] K. Habel, M. Viviani, E. Denarié, E. Brühwiler, Development of the mechanical properties of an Ultra-High Performance Fiber Reinforced Concrete (UHPFRC), Cement and Concrete Research, 36 (2006) 1362-1370.

[41] N. Van Tuan, G. Ye, K. van Breugel, O. Copuroglu, Hydration and microstructure of ultra high performance concrete incorporating rice husk ash, Cement and Concrete Research, 41 (2011) 1104-1111.

[42] P. Shen, H. Zheng, D. Xuan, J.-X. Lu, C.S. Poon, Feasible use of municipal solid waste incineration bottom ash in ultra-high performance concrete, Cement and Concrete Composites, 114 (2020).

[43] BS EN 1015-3/A2, Methods of test for mortar for masonry - Part 3: Determination of consistence of fresh mortar (by flow table), British Standard Institution, (2007).

[44] M.A.A. Aldahdooh, N. Muhamad Bunnori, M.A. Megat Johari, Evaluation of ultra-high-performance-fiber reinforced concrete binder content using the response surface method, Materials & Design (1980-2015), 52 (2013) 957-965.

[45] R. Snellings, K.L. Scrivener, Rapid screening tests for supplementary cementitious materials: past and future, Materials and Structures, 49 (2015) 3265-3279.

[46] H.A. Ali, D. Xuan, C.S. Poon, Assessment of long-term reactivity of initially lowly-reactive solid wastes as supplementary cementitious materials (SCMs), Construction and Building Materials, 232 (2020) 117192.

[47] X. Li, R. Snellings, M. Antoni, N.M. Alderete, M. Ben Haha, S. Bishnoi, Ö. Cizer, M. Cyr, K. De Weerdt, Y. Dhandapani, J. Duchesne, J. Haufe, D. Hooton, M. Juenger, S. Kamali-Bernard, S. Kramar, M. Marroccoli, A.M. Joseph, A. Parashar, C. Patapy, J.L. Provis, S. Sabio, M. Santhanam, L. Steger, T. Sui, A. Telesca, A. Vollpracht, F. Vargas, B. Walkley, F. Winnefeld, G. Ye, M. Zajac, S. Zhang, K.L. Scrivener, Reactivity tests for supplementary cementitious materials: RILEM TC 267-TRM phase 1, Materials and Structures, 51 (2018).

[48] BS EN 12390-7, Testing hardened concrete Part 7: Density of hardened concrete, British Standard Institution, (2019).

[49] BS EN 12390-5, Testing hardened concrete Part 5: Flexural strength of test specimens, British Standard Institution, (2019).

[50] BS EN 12390-3, Testing hardened concrete Part 3: Compressive strength of test specimens, British Standard Institution, (2019).

[51] ASTM E1050-19, Standard test method for impedance and absorption of acoustical materials using a tube, two microphones and a digital frequency analysis system, American Society of Testing Materials, (2019).

[52] ASTM E2611-19, Standard test method for normal incidence determination of porous material acoustical properties based on the transfer matrix method, American Society of Testing Materials, (2019).

[53] R.B. Polder, Test methods for on site measurement of resistivity of concrete — a RILEM TC-154 technical recommendation, Construction and Building Materials, 15 (2001) 125-131.

[54] ASTM C1585-13, Standard test method for measurement of rate of absorption of water by hydraulic-cement concretes, American Society of Testing Materials, (2013).

[55] J.-X. Lu, C.S. Poon, Improvement of early-age properties for glass-cement mortar by adding nanosilica, Cement and Concrete Composites, 89 (2018) 18-30.

[56] Y. Wu, J.-Y. Wang, P.J.M. Monteiro, M.-H. Zhang, Development of ultra-lightweight cement composites with low thermal conductivity and high specific strength for energy efficient buildings, Construction and Building Materials, 87 (2015) 100-112.

[57] S. Ng, B.P. Jelle, L.I.C. Sandberg, T. Gao, Ó.H. Wallevik, Experimental investigations of aerogel-incorporated ultra-high performance concrete, Construction and Building Materials, 77 (2015) 307-316.

[58] J.-X. Lu, Y. Zhou, P. He, S. Wang, P. Shen, C.S. Poon, Sustainable reuse of waste glass and incinerated sewage sludge ash in insulating building products: Functional and durability assessment, Journal of Cleaner Production, 236 (2019) 117635.

[59] S.E.S. Mendes, R.L.N. Oliveira, C. Cremonez, E. Pereira, E. Pereira, R.A. Medeiros-Junior, Electrical resistivity as a durability parameter for concrete design: Experimental data versus estimation by mathematical model, Construction and Building Materials, 192 (2018) 610-620.

[60] B.B. Hope, A.K. Ip, D.G. Manning, Corrosion and electrical impedance in concrete, Cement and Concrete Research, 15 (1985) 525-534.

[61] M. Kamali, A. Ghahremaninezhad, Effect of glass powders on the mechanical and durability properties of cementitious materials, Construction and Building Materials, 98 (2015) 407-416.

[62] O. Sengul, Use of electrical resistivity as an indicator for durability, Construction and Building Materials, 73 (2014) 434-441.

[63] R. Polder, C. Andrade, B. Elsener, Ø. Vennesland, J. Gulikers, R. Weidert, M. Raupach, Test methods for on site

measurement of resistivity of concrete, Materials and Structures, 33 (2000) 603-611.

[64] M.G. Sohail, R. Kahraman, N. Al Nuaimi, B. Gencturk, W. Alnahhal, Durability characteristics of high and ultra-high performance concretes, Journal of Building Engineering, 33 (2021).

[65] B. Sabir, S. Wild, M. O'farrell, A water sorptivity test for martar and concrete, Materials Structures, 31 (1998) 568-574.

[66] S. Kelham, A water absorption test for concrete, Magazine of Concrete Research, 40 (1988) 106-110.

[67] C. Hall, Water sorptivity of mortars and concretes: a review, Magazine of Concrete Research, 41 (1989) 51-61.

[68] P.K. Mehta, P.J.M. Monteiro, Concrete: Microstructure, Properties and Materials, McGraw-Hill, Third edition, USA, New York, (2006).

[69] K. Scrivener, R. Snellings, B. Lothenbach, A practical guide to microtructral analysis of cementitious materials, CRC Press, New York, USA, (2016).

[70] E. Tajuelo Rodriguez, K. Garbev, D. Merz, L. Black, I.G. Richardson, Thermal stability of C-S-H phases and applicability of Richardson and Groves' and Richardson C-(A)-S-H(I) models to synthetic C-S-H, Cement and Concrete Research, 93 (2017) 45-56.

[71] K. Garbev, M. Bornefeld, G. Beuchle, P. Stemmermann, Cell dimensions and composition of nanocrystalline calcium silicate hydrate solid solutions. Part 2: X‐ray and thermogravimetry study, Journal of the American Ceramic Society, 91 (2008) 3015-3023.

[72] K.K. Aligizaki, Pore structure of cement-based materials: testing, interpretation and requirements, CRC Press, London, 2006.

[73] M. Lopez, L.F. Kahn, K.E. Kurtis, Characterization of elastic and time-dependent deformations in high performance lightweight concrete by image analysis, Cement and Concrete Research, 39 (2009) 610-619.

[74] K.-S. Chia, X. Liu, J.-Y.R. Liew, M.-H. Zhang, Experimental study on creep and shrinkage of high-performance ultra lightweight cement composite of 60MPa, Structural Engineering and Mechanics, 50 (2014) 635-652.

[75] N.U. Kockal, T. Ozturan, Optimization of properties of fly ash aggregates for high-strength lightweight concrete production, Materials & Design, 32 (2011) 3586-3593.

[76] P. Shafigh, M.Z. Jumaat, H.B. Mahmud, U.J. Alengaram, A new method of producing high strength oil palm shell lightweight concrete, Materials & Design, 32 (2011) 4839-4843.

[77] R. Ahmmad, M.Z. Jumaat, U.J. Alengaram, S. Bahri, M.A. Rehman, H.b. Hashim, Performance evaluation of palm oil clinker as coarse aggregate in high strength lightweight concrete, Journal of Cleaner Production, 112 (2016) 566-574.

[78] M. Aslam, P. Shafigh, M. Alizadeh Nomeli, M. Zamin Jumaat, Manufacturing of high-strength lightweight aggregate concrete using blended coarse lightweight aggregates, Journal of Building Engineering, 13 (2017) 53-62.

[79] M.C.S. Nepomuceno, L.A. Pereira-de-Oliveira, S.F. Pereira, Mix design of structural lightweight self-compacting concrete incorporating coarse lightweight expanded clay aggregates, Construction and Building Materials, 166 (2018) 373-385.

[80] F. Sajedi, P. Shafigh, High-strength lightweight concrete using Leca, silica fume, and limestone, Arabian Journal for Science and Engineering, 37 (2012) 1885-1893.

[81] H. Zhou, A.L. Brooks, Thermal and mechanical properties of structural lightweight concrete containing lightweight aggregates and fly-ash cenospheres, Construction and Building Materials, 198 (2019) 512-526.

[82] Z. Kammoun, A. Trabelsi, A high-strength lightweight concrete made using straw, Magazine of Concrete Research, 72 (2020) 460-470.

[83] A. Trabelsi, Z. Kammoun, Mechanical properties and impact resistance of a high-strength lightweight concrete incorporating prickly pear fibres, Construction and Building Materials, 262 (2020).

[84] A. Dixit, S.D. Pang, S.-H. Kang, J. Moon, Lightweight structural cement composites with expanded polystyrene (EPS) for enhanced thermal insulation, Cement and Concrete Composites, 102 (2019) 185-197.

[85] T. Wu, X. Yang, H. Wei, X. Liu, Mechanical properties and microstructure of lightweight aggregate concrete with and without fibers, Construction and Building Materials, 199 (2019) 526-539.

[86] G. Xiong, C. Wang, S. Zhou, X. Jia, W. Luo, J. Liu, X. Peng, Preparation of high strength lightweight aggregate concrete with the vibration mixing process, Construction and Building Materials, 229 (2019) 116936.

[87] Y. Zhou, B. Xi, L. Sui, S. Zheng, F. Xing, L. Li, Development of high strain-hardening lightweight engineered cementitious composites: Design and performance, Cement and Concrete Composites, 104 (2019) 103370.

[88] F.B.d. Souza, O.R.K. Montedo, R.L. Grassi, E.G.P. Antunes, Lightweight high-strength concrete with the use of waste cenosphere as fine aggregate, Matéria, 24 (2019).

[89] S. Gupta, H.W. Kua, Application of rice husk biochar as filler in cenosphere modified mortar: Preparation, characterization and performance under elevated temperature, Construction and Building Materials, 253 (2020) 119083.

[90] K.J. Krakowiak, R.G. Nannapaneni, A. Moshiri, T. Phatak, D. Stefaniuk, L. Sadowski, M.J. Abdolhosseini Qomi, Engineering of high specific strength and low thermal conductivity cementitious composites with hollow glass microspheres for high-temperature high-pressure applications, Cement and Concrete Composites, 108 (2020) 103514.

[91] A.L. Brooks, H. Zhou, D. Hanna, Comparative study of the mechanical and thermal properties of lightweight cementitious composites, Construction and Building Materials, 159 (2018) 316-328.

[92] N. Kabay, A.B. Kizilkanat, B. Akturk, Y. Kahraman, Lightweight cement-based composites incorporating hollow glass microspheres: Fresh and hardened state properties, Teknik Dergi, 33 (2020) 1-25.

[93] W. Zhang, X. Yao, T. Yang, C. Liu, Z. Zhang, Increasing mechanical strength and acid resistance of geopolymers by incorporating different siliceous materials, Construction and Building Materials, 175 (2018) 411-421.

[94] F. Aslani, L. Wang, Development of strain ‐ hardening lightweight engineered cementitious composites using hollow glass microspheres, Structural Concrete, 21 (2019) 673-688.

[95] A.N. Al-Gemeel, Y. Zhuge, O. Youssf, Use of hollow glass microspheres and hybrid fibres to improve the mechanical properties of engineered cementitious composite, Construction and Building Materials, 171 (2018) 858-870.

[96] A. Hanif, Z. Lu, Z. Li, Utilization of fly ash cenosphere as lightweight filler in cement-based composites – A review, Construction and Building Materials, 144 (2017) 373-384.

[97] M.L. Torres, P.A. García-Ruiz, Lightweight pozzolanic materials used in mortars: Evaluation of their influence on density, mechanical strength and water absorption, Cement and Concrete Composites, 31 (2009) 114-119.